Towards a better understanding of the geochemical proxy record of complex carbonate archives

M. Mueller[a], B. F. Walter[b,c,d], R. J. Giebel[e,f], A. Beranoaguirre[c,d,g], P. K. Swart[h], C. Lu[h], S. Riechelmann[a], A. Immenhauser[a,i]

[a] Institute for Geology, Mineralogy and Geophysics, Ruhr-Universität Bochum. Universitätsstraβe 150, 44801 Bochum, Germany

[b] Eberhard Karls University Tübingen, Petrology and Mineral Resources, Schnarrenbergstraße 94-96, 72074 Tübingen, Germany

[c] Karlsruhe Institute for Technology, Chair of Economic Geology and Geochemistry, Adenauering 20b, 76131 Karlsruhe, Campus South, Germany

[d] Laboratory for Environmental and Rawmaterial Analyses (LERA), Adenauerring 20b, 76131, Karlsruhe, Campus South, Germany

[e] Technische Universität Berlin, Ernst-Reuter-Platz 1, 10587 Berlin, Germany

[f] University of the Free State, 250 Nelson-Mandela-Drive, Bloemfontein 9300, South Africa

[g] Frankfurt Isotope and Element Research Center, Goethe-UniversitätFrankfurt, Altenhöferallee 1, 60438 Frankfurt am Main, Germany

[h] Department of Marine Geosciences, Rosenstiel School of Marine, Atmospheric and Earth Sciences, University of Miami, Miami, 33149, FL, USA

[i] Fraunhofer Research Institution for Energy Infrastructures and Geothermal Systems IEG. Am Hochschulcampus 1, 44801 Bochum, Germany

[*] Corresponding author: mathias.mueller-l1y@rub.de

Digital supplement S1

3.   Methodology

3.4 Fluid inclusion thermometry

Microthermometric analyses on fluid inclusions were carried out using a Linkam THMS600 heating-freezing stage at the LERA facilities at Karlsruhe Institute for Technology (KIT). Double-polished thick sections (100 to 150 µm) for fluid petrography were prepared. The petrographic relation of each fluid inclusion assemblage was carried out by optical and cathodoluminescence microscopy, following the approach of Goldstein and Reynolds (1994). The documented fluid inclusion assemblages (FIA) were classified as (i) primary inclusions, which are situated on growth zones (p), (ii) pseudo-secondary (ps), (iii) secondary (s), and (iv) isolated inclusions with no genetic relationship (iso; Walter et al., 2015). For each analysis, three repeated heating and freezing cycles were performed to document the final dissolution temperature of ice ($T_{m, ice}$) and hydrohalite ($T_{m, hh}$) and the homogenization temperature (T_h). For further genetic interpretations, only fluid inclusions were considered, for which a triplet measurement varies between <0.1 °C for $T_{m, ice}$ and $T_{m, hh}$ and <1 °C for T_h. All inclusions and the corresponding data were checked for evidence of post-entrapment modifications. Some inclusion analyses resulted in microthermometric data, which indicated a metastable absence of hydrohalite due to the system-related phase diagram NaCl-H_2O-$CaCl_2$ (Steele-MacInnis et al., 2011). Such inclusions were excluded from the data presentation and interpretation because no geologically correct information can be gathered from them. Synthetic quartz-hosted H_2O, H_2O-NaCl, and H_2O-CO_2 standard inclusions (SynFlinc Standard collection) were used for temperature calibration once a day.

Quantification of molar Ca/(Na+Ca) ratios in the ternary NaCl-$CaCl_2$-H_2O system were performed with the Excel-based calculation program of Steele-MacInnis et al. (2011). The volume fraction of each fluid inclusion was visually estimated based on published volume proportion tables (Shepherd et al., 1985). The volume fraction notation used is based on the phase assemblage at room temperature, aqueous liquid (Lx, numerical subscription refers to the volume percentage of aqueous liquid), carbonic liquid (Lc), vapor (V), and solid (S) (Shepherd et al., 1985; Bakker and Diamond, 2006; Walter et al., 2019). Pressure correction of the T_h values and density calculation was performed by use of the HOKIEFLINCS_H2O-NACL program of Steele-MacInnis et al. (2011), assuming lithostatic conditions with a depth of the water column inferred from the

cumulated overburden lithology thicknesses and maximum paleo-depth of 6,500 m (Drozdzewski and Wrede, 1994; Littke et al. 2000; Götte, 2004). Lithostatic conditions are assumed because of the cover by subsequently deposited Middle/Late Devonian sediments predating dolomitization and tectonic processes. Raman Microspectroscopy was performed, but no signal for semiqualitative analyses was received due to the small inclusion sizes.

3.5 Crush leach analysis

20 samples with one dominant fluid type were selected for bulk fluid crush-leach analyses. About 2 grams of carbonate with a grain size of 0.5 to 1 mm were hand separated, and visible impurities were removed. The separates were washed for 3 hours in Milli-Q water at 60-70 °C. Subsequently, the samples were washed for one week with ultrapure water, changing the water twice a day. These pre-treated samples were dried and crushed to a fine powder in an agate mortar. 20 ml of Milli-Q water was added to the powder in the agate mortar, whereas 10 ml was used for IC and 10 ml for ICPMS. To suppress the adsorption of doubly-charged cations, crush-leach solutions were acidified with supra pure HNO_3 (Köhler et al., 2008; Ladenburger et al., 2020). The loaded solution was injected into a Methrom 930 Compact IC Flex chromatography system equipped with an 858 Professional Sample Processor and a Metrosep A Supp 5 column to quantify anions (F, Cl, Br, J, NO_3, PO_4, and SO_4). To inject the solutions into the Methrom 858 Professional Sample Processor, we used disposable syringe filters CROMAFILE®Xtra RC-20/25 for anions (Ladenburger, 2020). Blank runs were carried out before and after each analysis, and defined standard solutions were regularly analyzed to monitor the reproducibility and precision of the measurements. Uncertainties were usually smaller than 15%, and effective detection limits were generally <10 mg/l.

Trace element concentrations in the crush-leach solutions were measured with an iCAP RQ ICP-M (Thermo Fisher Scientific), which is equipped with a collision cell to eliminate polyatomic clusters. An ICP multi-element standard solution (Merck, Certipur) was used for calibration and quality checks. [103]Rh and [115]In were used as internal standards for all measurements. The certified reference water CRM-TMDW-A (High-Purity standards, Inc.) was used to check for the precision and accuracy of the measurement procedure. Accuracy was between 1 and 8% in the measured sample batch. Absolute element concentrations in the original (non-diluted) fluid compositions were calculated using the microthermometry chlorine results as internal standard.

3.6 Geochemistry

Mineralogy of individual cement phases was analysed using powder X-Ray Diffraction (PXRD). To quantify the minerals present, 70–100 mg of powder was drilled from the samples with a handheld Dremel. Sampling locations within individual phases were based on previous petrographic evaluation using normal, polarised and cathodoluminescence microscopy. Sample powders were homogenously distributed on a silicon sample carrier, before mounting and aligning them on a rotating goniometer head. Measurements were performed on a PANalytical EMPYREAN diffractometer using copper radiation ($\lambda 1 = 0.154$ Å) equipped with a PIXcel1D detector (Medipix2 collaboration, Ruhr-University, Bochum, Germany). Scanning range of 2-Theta was 5 to 80°, with a step size of 0.0131°, and a duration of 598.9 ms. Phases were identified using the software X'Pert HighScore Plus (PANalytical B.V.).

Element concentrations, carbon- and oxygen-isotope values ($\delta^{13}C$ and $\delta^{18}O$), and $^{87}Sr/^{86}Sr$ ratios were analysed at Ruhr-University Bochum. For $\delta^{13}C$ and $\delta^{18}O$ analysis, 90-110 µg of carbonate sample powder was reacted with phosphoric acid at 70°C before analysis. Isotope values were determined using a MAT 253 (Thermo Fisher Scientific) continuous flow isotope ratio mass spectrometer (CF-IRMS) coupled with a ConFloIV and a GasBenchII. Values are reported in ‰ relative to the VPDB standard. Measurement error is reported as 1σ standard deviation (SD). The certified standards IAEA-603 and NBS 18 were used for data correction. The 1σ-reproducibility of the internal limestone standard was 0.05 ‰ for $\delta^{13}C$ and 0.08 ‰ for $\delta^{18}O$ (n=134, 2021-2023) and 0.06 ‰ for $\delta^{13}C$ and 0.11 ‰ for $\delta^{18}O$ (n=80, 2021-2023) for the internal dolomite standard.

Elemental concentrations (Ca, Mg, Sr, Fe, Mn) were measured for all carbonate phases. Samples were run by dissolving approximately 1.5 mg of sample powder in 1 ml 3M HNO_3 for 24 h at room temperature before diluted with 2 ml deionised water. Concentrations were determined by inductively coupled plasma optical emission spectrometry (ICP-OES, iCAP 6500 DUO, Thermo Fisher Scientific). Measurement error is reported as 1σ standard deviation (SD). The long-term 1σ-reproducibility of the certified standards BCS-CRM512 (dolomite, Bureau of Analysed Samples Ltd) and BCS-CRM513 (limestone; Bureau of Analysed Samples Ltd) is 0.3 wt.% and 0.6 wt.% for Ca, 0.2 wt.% and 0.002 wt.% for Mg, 0.002 wt.% and 0.0003 wt.% for Sr, 0.001 wt.% and 0.0009 wt.% for Fe, and 0.0001 wt.% and 0.0002 wt.% for Mn, respectively (n=116; 2019-2022).

Strontium-isotope ratio analyses were performed by dissolving between 0.3 to 16.3 mg (to receive a Sr content of 400 ng per sample) of sample powder in 1 ml 6M HCl and dried on a hot plate at 90°C before being re-dissolved in 0.4 ml 3M HNO_3. PFA columns filled with TrisKem Sr ion exchange resin (100-150 mesh) were used to collect the Sr fraction with 2 ml of deionised water. Subsequently, samples are dried on a hot plate at 90°C and re-dissolved in 1 ml of a H_2O_2-HNO_3 to remove organic remains. Samples were then evaporated on a hot plate at 60°C and re-dissolved in 0.4 ml 6M HCl. After evaporation at 90°C, samples were re-dissolved in 1 µl of ionisation-enhancing solution (after Birck 1986) and loaded on Re single filaments. Isotope ($^{87}Sr/^{86}Sr$) ratios were analysed by thermal ionisation mass spectrometry (TIMS) TI-BOX (formerly MAT 262; Spectromat). Measurement error is reported as 2σ standard error (SE). The long-term reproducibility of NIST NBS 987 and USGS EN-1 is $^{87}Sr/^{86}Sr = 0.710247 \pm 0.000002$ 2σ SE (n=181; 2017-2022) and $^{87}Sr/^{86}Sr = 0.709168 \pm 0.000003$ 2σ SE (n = 146; 2017-2022), respectively.

3.7 Clumped isotope analysis

3.7.1 Isotope analysis

Samples for clumped isotope analysis were taken from single-phase powder samples. Each measurement of the Δ_{47} value requires ~8 mg of carbonate to produce sufficient CO_2 for analysis. Samples were weighed into copper reaction boats and reacted using the common acid bath at 90 °C, using concentrated phosphoric acid (density = 1.95 g/cm³) on the University of Miami Stable Isotope Laboratory's vacuum line. Liberated gas was continuously frozen with liquid nitrogen in a U-trap throughout the reaction to minimize the potential of exchange between CO_2 and water released from the reaction with acid. Calcite samples reacted to completion within 30 min, dolomite samples required longer reaction times, typically reacting for 45 min to 1 h before bubbles were no longer produced. Reaction times were unaffected by carbonate content. The H_2O was separated from CO_2 using a -90 °C methanol slush. Volatile organic compounds and other contaminants were removed by passing the gas through a Porapak^{TM} Q adsorbent trap (passively, no He carrier gas) chilled in methanol between -20 and -30 °C gas was frozen in a trap cooled with LN_2 after passing through to facilitate 100% extraction of gas. Gas samples are frozen into a glass vessel and transferred to a Thermo-253 Plus mass spectrometer.

The CO_2 analysis was performed in analytical sessions, consisting of six blocks of measurements, each including 14.5 alternations between the reference and the sample gases. Samples from both carbonates and equilibrated gases were measured at a signal voltage of 12 V with approximately equal volumes of gas on both the reference and sample bellows. Integration time was 14 seconds with a 15 second delay time before the start of the measurement. Before and after each block the background was measured (four alterations before and four alterations after) using the approach outlined by He et al. (2012). As the signal on the major beam was rebalanced to 12 V between each block, this resulted in a total analytical time on each sample of ~ 2.2 to 2.4 hours on each sample, depending upon the time taken to rebalance the signal. The total integration time on peaks was 2,521 seconds. Based on the calculations of Merritt and Hayes (1994), this provided a shot noise estimate of 0.008 ‰ for Δ_{47} at 12 V. Data reduction and normalization for the calculation of the raw Δ_{47} value followed the framework of Huntington et al. (2009) and the recommendations of Daëron et al. (2016). The final Δ_{47} values ($\Delta_{47\text{-processed}}$) were calibrated by using both the CDES (Carbon Dioxide Equilibrated Scale) of Dennis et al. (2011) and I-CDES (Intercarb CDES) of Bernasconi et al. (2021). The CDES was established by using CO_2 gas contained within sealed quartz tubes heated to 1000°C for several hours and CO_2 gas equilibrated with a single internal laboratory water standard sealed within a Pyrex tube and held within a water bath at 25 and 50°C for 48 hrs. All details of this method are described by Murray et al. (2016). The equilibrated gases were analyzed approximately every 3-4 weeks and the ETH standards (ETH-1, 2, 3, and 4) every seven days. Changes in the intercepts and slopes of the Δ_{47} and δ^{47} values from the equilibrated gases were interpolated to correct the drift during this period. For the I-CDES framework, the ETH standards were used to correct the Δ_{47} values following the InterCarb method in Bernasconi et al. (2018) and Bernasconi et al. (2021). The ETH values are averaged over 15-day and 30-day windows. The 30-day window is equivalent to the interval of the EG and includes 8 to 12 measurements for ETH-1 and 2 standards.

To detect the short-term fluctuations of the slope and intercept suggested by Bernasconi et al. (2018), the 15-day window always consists of 4 to 6 samples of ETH -1 and 2. The linearity correction used ETH-1 and -2 with the "true values" from Bernasconi et al. (2021). The transfer function is based on measurements of four carbonate standards (ETH-1, 2, 3, and 4). The reacting samples are regarded as the unknown values for comparing the EG and ETH frameworks.

The $\delta^{13}C$ and $\delta^{18}O$ values of the reference gas were determined by analyzing NBS-19 (National Bureau of Standards), and data for the samples reported relative to Vienna Pee Dee Belemnite (V-PDB) using the conventional notation. The $\delta^{18}O$ values for dolomite have been corrected by 0.8‰ to account for the differential fractionation of ^{18}O during the formation of dolomite when compared to calcite (Sharma and Clayton, 1965).

Calculation of temperature and fluid $\delta^{18}O$ values: Calculation of temperatures was made using the calibration of Swart et al. (2019):

$$\Delta_{47} = 0.0392 * 10^6/T^2 + 0.158 \,.$$

Calculation of the $\delta^{18}O$ values of fluids ($\delta^{18}O_{fl}$) was performed using the equation of Kim and O'Neil (1997) and Horita (2014) for calcite and dolomite respectively.

3.9. Trace elements in quartz

In-situ trace element compositions of quartz were obtained by laser ablation inductively coupled plasma mass spectrometry (LA-ICP-MS) using a Teledyne Analyte Excite+ ArF (193 nm) excimer laser ablation system coupled to a Thermo-Scientific Element XR sector field mass spectrometer at LERA, KIT. For analysis, a laser spot size of 65 µm, a pulse rate of 10 Hz and an energy density of 11.0 J/cm^2 were used. Samples were ablated in a He stream of ~0.5 l/min to which 8-11 ml/min N$_2$ and ~0.85 l/min Ar were added directly after the ablation cell. All analyses were performed at low oxide production rates (UO+/U+ < 0.1%) and robust plasma conditions (sensitivity ratio U+/Th+ = 1.0) along transects in quartz growth direction. All data were acquired and reduced in blocks of 30 unknowns bracketed by NIST-612 glass reference material. Data were processed using the Iolite data reduction software (Paton et al. 2011) using NIST-612 for external calibration (values of Pearce et al., 1997). All signals were normalized to ^{29}Si as an internal standard using 100 wt.% SiO$_2$ for data reduction of quartz analyses. To monitor accuracy, NIST-614 glass was analyzed as an unknown and yielded trace element contents of Be = 0.76 ± 0.6 ppm (2σ), Ti = 3.3

± 0.1 ppm (2σ), Co 0.77 ± 0.02 ppm (2σ), Ni = 1.10 ± 0.04 ppm (2σ), Zn = 2.5 ± 0.1 ppm (2σ), Ge = 0.99 ± 0.08 ppm (2σ), Rb = 0.87 ± 0.03 ppm (2σ), Nb = 0.84 ± 0.02 ppm (2σ), Mo = 0.83 ± 0.03 ppm (2σ), In = 0.84 ± 0.04 ppm (2σ), Sb = 0.76 ± 0.02 ppm (2σ), W = 0.80 ± 0.03 ppm (2σ), Au = 0.53 ± 0.02 ppm (2σ), Pb = 2.4 ± 0.1 ppm (2σ) and Bi = 0.58 ± 0.01 ppm (2σ), which agree with published values of Jochum et al. (2011).

4.   Results

4.1 Cement stratigraphy

A paragenetic succession of the carbonates in the Steltenberg quarry was established from field observations (Figs 2 and 3), thin section data (n = 127), and cathodoluminescence analysis (Figs 4-6). Here, we complement the basic version of this complex paragenetic sequence that we presented in Pederson et al. (2021) with new data. The used dolomite terminology follows Sibley and Gregg (1987).

The Devonian Massenkalk limestone (MK limestone) precursor is characterised by fine- to medium-grained depositional facies, which include fossil brachiopods (*Stringocephalus burtini*), sponges, corals, bivalves, and crinoids. This phase generally has bright red luminescence (Fig. 4A, B). Occasionally, medium- to coarse crystalline euhedral dolomite rhombs occur in the rock matrix. Pores and vugs are often filled by marine or burial cements. The precursor limestone was partially or fully replaced by three dolomite phases and several hydrothermal and meteoric calcite cements as well as hydrothermal quartz, sulphides, and iron oxides. The first dolomite phase Dol 1 is divided into a dark grey fine to medium grained planar-s dolomite with patchy red to pale orange luminescence (Dol 1A; Fig. 4C, D) and a white nonplanar coarse crystalline nonplanar saddle dolomite (Dol 1B; Fig. 4C, D). Locally, the limestone beds are cut by sets of calcite veins likely associated to early Variscan faulting and deformation (VFD LMC). These are characterized by patchy red-orange luminescence and their thickness varies from submillimetre to centimetres.

The second dolomite phase Dol 2 is divided into a brownish fine to medium crystalline planar-s to nonplanar matrix dolomite (Dol 2A; Fig. 4E, F) and a beige nonplanar coarse crystalline nonplanar saddle dolomite (Dol 2B; Fig. 4G, H) with sweeping extinction and red-orange patchy luminescence. It occurs in ENE-WSW trending mm to dm sized veins or as vug-filling cement.

The veins often contain breccia clasts of µm to dm size (Breccia 1). In places, Dol 1 and Dol 2 were dedolomitized. This phase Dedol 1 is best visible in breccia clasts and vugs, retained dolomite crystal morphology and is non-luminescent. Dolomite Dol 2 and Dedol 1 are typically overgrown by white blocky macrocrystalline LMC 1, a dark red luminescent calcite cement, which forms in vugs and around mm to m sized breccia clasts (Breccia 2) in vein swarms up to several meters in diameter (Figs 2B, D, 4G, H). Similar to Dol 2, the LMC 1 veins are ENE-WSW trending and show a clear relation to the Variscan thrust fault zone.

In places, laminated dolomite cements (Laminite 1, Fig. 3G) occur in vicinity to the NNW-SSE trending Post-Variscan fault zone within filled or later collapsed karst cavities. They have a patchy bright red luminescence and consist of a fine-grained skeletal framework, which forms mm-sized bladed crystals (Fig. 6A, B). These are usually intercalated between µm to meter thick layers of brown clayey dolopackstones with a similar patchy bright red luminescence (Fig. 6A, B) and up to dm-sized blocky low Mg calcite (LMC 2) characterized by clear to patchy bright orange luminescence (Fig. 6C, D). The third and last preserved dolomite phase Dol 3 is divided into a medium to coarse crystalline nonplanar matrix dolomite (Dol 3A; Fig. 5A-D) and a coarse crystalline vug-filling nonplanar saddle dolomite (Dol 3B; Fig. 5E, F) characterised by dark to bright red patchy luminescence. Dolomite Dol 3 occurs in NNW-SSE trending veins, which crosscut Dol 2 veins in places, and its formation is clearly related to the NNW-SSE trending Post-Variscan fault zone. In the vicinity of the Post-Variscan fault zone, Dol 3 growth continued between breccia clasts after another breccia was formed (Breccia 3). At a later stage after its formation, most Dol 3 was partly or fully dedolomitized. This Dedol 2 is micro-to macrocrystalline, mostly retained dolomite crystal morphology but is patchy dark red to yellow luminescent (Fig. 5G, H). In places, Dol 3, the Breccia 3 clasts, and Dedolomites were heavily oxidized and contain iron oxides (hematite, goethite, limonite, Figs 2E and 3E). Dolomite Dol 3 and dedolomite Dedol 2 are often overgrown in vugs by fine to coarse crystalline quartz phases (Qz 1 and Qz 2; Fig. 5E-H) with pale green to dark blue luminescence. In places, these phases are overgrown by non luminescent sulphides (pyrite, chalcopyrite). Simultaneously (LMC 2 and LMC 3) and subsequent (LMC 4A to LMC 10) to dolomite, iron oxide, quartz, and sulphide precipitation, a series of calcite cements precipitated. These are divided into several low-Mg calcite phases (LMC 2 to LMC 10), of which LMC 2 to LMC 4 form vein swarms in NNW-SSE direction, indicating a relation to the Post-Variscan fault zone. The calcite cement phase LMC 3 forms macrocrystalline radial to blocky

crystals up to several dm size and has dark red luminescence without visible zoning (Fig. 6E, F). Microscopically and macroscopically, fibrous LMC 3 crystals often show features of rapid skeletal growth (Fig. 6F). Locally, LMC 3 contains breccia clasts up to several dm, which are overgrown by up to few dm sized crystals. It is prominent in the main strand of the Post-Variscan fault zone. Along grain boundaries, yellow luminescent LMC 4A overprints LMC 3 and older dolomite/calcite phases (Figs 4H, 6F). In places, this phase is overgrown by macrocrystalline blocky LMC 4B, which forms non-luminescent to yellow cm-sized crystals. In the main strand of the Post-Variscan fault zone it is cut by a quartz gangue (Qz 3) with intensely zoned blue-green luminescence. The phase LMC 5 forms dog tooth to radial-shaped cm to dm-sized clear to cloudy brownish crystals in veins and mm to cm sized white blocky crystals in breccias from the Post-Variscan fault zone. The phase is characterized by a bright orange to patchy phase A and a patchy bright yellow phase B, which often overprints older phases (Fig. 4H; 5B; 6F). The phase LMC 6 consists of subphases A-D, which are characterized by patchy red to orange (LMC 6A, C; Fig. 6G, H) and dark to bright red orange luminescence (LMC 6B, D; Fig. 6G, H). The phase forms macrocrystalline brown to white blocky crystals up to 1 cm size. The phase occurs in vein swarms that crosscut the Post-Variscan fault zone, indicating a younger tectonic origin (Fig. 2E). The micro to macrocrystalline phase LMC 7 consists of an inner inclusion-rich and an outer inclusion-lean layer with patchy bright red (LMC 7A) and clear zoned red to orange luminescence. The phase LMC 8 is found as fracture-filling mm-sized blocky phase between breccia clasts in the vicinity of the Post-Variscan fault zone. It shows dark red to bright red luminescence and is zoned (Fig. 6A, B). The phase LMC 9 typically occurs as youngest phase in vugs on top of either the pre formed LMC phases or dolostones. Within the LMC phases, LMC 9 often altered pre-existing calcite phases by percolation through crystal and grain-boundaries (Fig. 6B). It forms skalenoedric millimetre to centimetre sized inclusion-lean crystals and has intrinsic dark blue to yellow zoned luminescence. The red luminescent phase LMC 10 forms botryoidal fibrous macrocrystalline aggregates and typically builds cement crusts in karst cavities.

4.3 Fluid inclusion data

To decifer the fluid evolution of a hydrothermal system, a detailed fluid-inclusion petrography is required which was performed using transmitted light microscopy (Goldstein and Reynolds, 1994; Walter et al., 2015). It was possible to gather data from primary, pseudo secondary, and isolated inclusions (n = 215 fluid inclusions in 55 fluid inclusion assemblages, FIA) in quartz and carbonate phases. Pseudo-secondary inclusions refer to healed fractures and therefore are per definition older than the overgrowing paragenetic cement generation. Primary inclusions are hosted on growth zones of carbonates. Primary fluid inclusions which occur on crystal growth zones are typically smaller (1-5 µm) than pseudosecondary assemblages (<5-20 µm) and usually do not show well developed inclusion walls. Please note that the very small fluid inclusion sizes and the transparence of the host minerals were the major challenge during the analyses which lead to a relatively low statistic for the individual FIAs. Nevertheless, it was possible to gather data of all important diagenetic phases of the study. Therefore, the presented data have to be treated with caution to avoid over-interpretation of individual compositions. Hence, the fluid characteristics will be discussed in a holistic manner. Homogenization was always into the liquid phase and volume fractions are always ~ 0.95 (L0.95V0.05). This indicates that no significant post-entrapment modification happened, which would be also reflected in single homogenization temperatures within a FIA that are higher than the rest. Moreover, no CO_2 and CH_4 were observed.

Fluid inclusions hosted by Dol 1A always show a metastable behavior. Therefore, no geological meaningful data was collected in this generation. In Dol 1B (n = 10), fluid inclusions are hosted on primary growth zones (n = 7) and in clusters (n = 3). These show T_h between 99 and 124 °C at salinities of 18.4 to 23.9 wt% $NaCl+CaCl_2$. In generation Dol 2A (n = 22), primary fluid inclusions (n = 13) and clusters (n = 9) show T_h between 63 and 131°C at salinities of 19.2 to 25.7 wt% $NaCl+CaCl_2$. Fluid inclusions hosted by Dol 2B (n = 37) exclusively occur as clusters in numerous samples. These have T_h of 97-127°C and salinities of 20.0 to 22.6 wt.% $NaCl+CaCl_2$. Primary fluid inclusions in LMC 1 (n = 10) have T_h of 195-224°C and salinites between 15.1-18.4 wt.% NaCl. Fluid inclusions in Dol 3A (n = 8) are metastable (primary inclusions; n = 4) with T_h between 81-83°C and clustered inclusions (n = 4) between 99-117°C. The latter bear salinities between 22.0 and 23.2 wt.% $NaCl+CaCl_2$. Fluid inclusions in Dol 3B (n = 18) contain T_h of 147-149°C (primary; n = 4)) at salinities of 20.4-22.0 wt.% $NaCl+CaCl_2$. Those fluid inclusions hosted in clusters (n = 14) contain lower T_h of 119-130°C at slightly lower but $CaCl_2$ lacking salinities of

20.6-21.7 $NaCl_{eq}$. The primary fluid inclusions in Laminite 1 (n = 9) contain T_h from 207-221°C and very low salinities between 2.9 and 6.4 wt.% $NaCl_{eq}$. Those fluids hosted in Dedol 2 (n = 6) occur in clusters with T_h of 122-132°C and salinities of 6.8-14.3 wt.% $NaCl_{eq}$. Fluid inclusions in Qz 2A (n = 11; 109-121°C, 21.7-22.8 wt.% $NaCl+CaCl_2$) and Qz 2B (n = 18; 89-124°C, 21.0-24.7 wt.% $NaCl+CaCl_2$) are primary (n = 22) or occur in clusters (n = 7). The fluid inclusions in LMC 2 were either metastable or too small for analysis, therefore, no data was collected in this generation. The primary fluid inclusions in LMC 3 (n = 24) have T_h between 76 and 94°C and show a bimodal salinity distribution (4.5-6.4 wt.% $NaCl+CaCl_2$ *versus* 22.3-24.3 wt.% $NaCl+CaCl_2$). Primary fluid inclusions in LMC 4 (n = 4) have T_h between 119 and 130°C and salinities between 5.2 and 5.9 wt. % $NaCl_{eq}$. Primary fluid inclusions in LMC 5 (n = 7) have T_h between 84 and 93°C and salinities between 24.3 and 26.1 wt.% $NaCl+CaCl_2$. Primary fluid inclusions in LMC 6 (n = 11) have T_h between 54 and 61°C and salinities between 17.2 and 20.1 wt.% $NaCl+CaCl_2$. Clustered inclusions (n = 4) have higher T_h of 156-191°C and similar salinities (15.1-17.9 wt. % $NaCl_{eq}$). Clustered inclusions in LMC 7 (n = 4) have T_h of 123-130°C and salinities between 16.7 and 18.1 wt. % $NaCl_{eq}$. Primary fluid inclusions in LMC 8 (n = 5) have T_h between 164 and 196°C and salinities between 15.2 and 17.1 wt. % $NaCl_{eq}$. In both LMC 9 and LMC 10 no fluid inclusions with a gas phase were found.

4.6 Isotope geochemistry

Stable $\delta^{13}C$ and $\delta^{18}O$ isotope values and $^{87}Sr/^{86}Sr$ ratios for all drilled cement phases are given in Table 2, where only the most important features are reported. Detailed tables including: (i) major and trace element concentrations; and (ii) $\delta^{13}C$ and $\delta^{18}O$ ranges, and $^{87}Sr/^{86}Sr$ in sample groups, are given in the digital appendix. The $\delta^{18}O$ values of 180 powder samples range from -13.9‰ (LMC 1) to -0.4‰ (Laminite 1), independent of mineralogy and age of formation. Among these, the MK limestone bulk host rock yields $\delta^{18}O$ values from -9.9 to -5.2‰ (mean of -7.1‰; n = 10). The paragenetically oldest dolomite phase Dol 1 (Dol 1A and Dol 1B) yields $\delta^{18}O$ values from -10.1 to -4.5‰ (mean of -7.4‰; n = 27). These data are similar to Dol 2 (Dol 2A and Dol 2B) samples, which yield $\delta^{18}O$ values from -9.8 to -5.4‰ (mean of -7.8‰; n = 25). In contrast, Dol 3 samples are enriched in ^{18}O relative to the other dolomites. These yield $\delta^{18}O$ values from -7.2 to -3.4‰ (mean of -5.7‰; n = 30) whereas Dol 3B samples are more enriched in ^{18}O than Dol 3A samples ($\delta^{18}O_{mean}$ Dol 3A = -7.1‰; n = 10); $\delta^{18}O_{mean}$ Dol 3B = -5.7‰; n = 20). The Laminite 1 dolomite

cement phases yield $\delta^{18}O$ values from -4.5 to -0.4‰ (mean of -2.3‰; n = 6). The Low Mg calcite phases LMC 1 to LMC 10 and Dedol 1/2 yield $\delta^{18}O$ values from -13.9 to -3.4‰ (mean of -6.8‰; n = 79).

The $\delta^{13}C$ values of all 180 powder samples range from -7.4‰ (Dedol 2) to +4.6‰ (Dol 3B). Among these, the MK limestone bulk host rock yields $\delta^{13}C$ values from +2.4 to +3.2‰ (mean of +2.8‰; n = 10). The paragenetically oldest dolomite phase Dol 1 (Dol 1A and Dol 1B) yields $\delta^{13}C$ values from +3.4 to +3.9‰ (mean of +3.6‰; n = 27). The Dol 2 (Dol 2A and Dol 2B) samples yield $\delta^{13}C$ values from +1.4 to +3.8‰ (mean of +3.2‰; n = 25). These are similar to Dol 3A samples, which yield $\delta^{13}C$ values from +3.2 to +3.8‰ (mean of +3.6‰; n = 10). In contrast, Dol 3B samples are depleted in ^{13}C relative to the other dolomites. These yield $\delta^{13}C$ values from -1.3 to +4.6‰ (mean of +1.5‰; n = 20). The Laminite 1 dolomite cement phases yield $\delta^{13}C$ values from -3.0 to -2.1‰ (mean of -2.6‰; n = 6). The Low Mg calcite phases LMC 1 to LMC 10 and Dedol 1/2 yield $\delta^{13}C$ values from -7.4 to +2.7‰ (mean of -0.9‰; n = 79).

The strontium isotope ratios (n = 38, Table 2) range between 0.707915 ± 0.000005 (pristine brachiopod shell) and 0.714721 ± 0.000006 (Laminite 1). The MK limestone host rock has a mean $^{87}Sr/^{86}Sr$ ratio of 0.708442 ± 0.000005 (n = 3). The dolomite Phases Dol 1 to Dol 3 plot between 0.708565 ± 0.000005 (Dol 3A) and 0.710021 (Dol 1) with a mean $^{87}Sr/^{86}Sr$ ratio of 0.709210 ± 0.000005 (n = 14). The Laminite 1 dolomite cement phases plot between 0.709028 ± 0.000005 (Lam 1 Dol cc, n = 1) and 0.714721 (Lam 1 clayey dolopackstone, n = 1). The Low Mg calcite phases LMC 1 to LMC 9 and Dedol 1/2 plot between 0.708757 ± 0.000005 (LMC 1) and 0.713170 ± 0.000005 (LMC 5) with a mean $^{87}Sr/^{86}Sr$ ratio of 0.710087 ± 0.000005 (n = 18). There is no clearly visible paragenetic trend and most phases plot between 0.7085 and 0.7100 (n = 28).

5.   References

Bakker, R.J. and Diamond, L.W., 2006. Estimation of volume fractions of liquid and vapor phases in fluid inclusions, and definition of inclusion shapes. *American Mineralogist*, **91**: 635–657. https://doi.org/10.2138/am.2006.1845

Bernasconi, S.M., Muller, I.A., Bergmann, K.D., et al., 2018. Reducing uncertainties in carbonate clumped isotope analysis through consistent carbonate-based standardization: *Geochem. Geophys. Geosys.*, **19**(9): 2895-2914. https://doi.org/10.1029/2017GC007385

Bernasconi, S.M., Daëron, M., Bergmann, K.D., Bonifacie, M., Meckler, A.N., Affek, H.P., Anderson, N., Bajnai, D., Barkan, E. and Beverly, E., 2021. InterCarb: a community effort to improve interlaboratory standardization of the carbonate clumped isotope thermometer using carbonate standards: *Geochem., Geophys., Geosys.*, **22**: e2020GC009588.

Birck, J.L. (1986). Precision K-Rb-Sr isotopic analysis: Application to Rb-Sr chronology. *Chemical Geology*, 56, 73–83. https://doi.org/10.1016/0009-2541(86)90111-7

Daëron, M., Blamart, D., Peral, M. and Affek, H.P., 2016. Absolute isotopic abundance ratios and the accuracy of Δ_{47} measurements: *Chemical Geology*, **442**: 83–96. https://doi.org/10.1016/j.chemgeo.2016.08.014

Dennis, K.J., Affek, H.P., Passey, B.H., Schrag, D.P. and Eiler, J.M., 2011. Defining an absolute reference frame for 'clumped' isotope studies of CO_2. *Geochimica et Cosmochimica Acta*, **75**: 7117–7131. https://doi.org/10.1016/j.gca.2011.09.025

Drozdzewski, G. and Wrede, V., 1994. Faltung und Bruchtektonik – Analyse der Tektonik im Subvariscikum. Fortschr. *Geol. Rheinl. Westfal.*, **38**: 7–187.

Goldstein, R.H. and Reynolds, T.J., 1994. Systematics of fluid inclusions in diagenetic minerals. Short Course 31. *Society of Economic Paleontologists and Mineralogists*, **31**: 199 p.

Götte, T., 2004. Petrographische und geochemische Untersuchungen zu den postvariszischen Mineralisationen im devonischen Massenkalk des nordwestlichen Rechtsrheinischen Schiefergebirges unter besonderer Berücksichtigung der Kathodolumineszenz. *Dissertation University of Bochum*, 186 p.

He, B., Olack, G.A. and Colman, A.S., 2012. Pressure baseline correction and high-precision CO_2 clumped-isotope ($\Delta47$) measurements in bellows and micro-volume modes: *Rapid Communications in Mass Spectrometry*, **26**: 2837–2853.

Horita, J., 2014. Oxygen and carbon isotope fractionation in the system dolomite–water–CO_2 to elevated temperatures. *Geochimica et Cosmochimica Acta* **129**: 111-124. https://doi.org/10.1016/j.gca.2013.12.027

Huntington, K. W., Eiler, J. M., Affek, H. P., Guo, W., Bonifacie, M., Yeung, L. Y., et al., 2009. Methods and limitations of 'clumped' CO_2 isotope (Δ_{47}) analysis by gas-source isotope ratio mass spectrometry: *Journal of Mass Spectrometry*, **44**(9): 1318–1329. https://doi.org/10.1002/jms.1614

Jochum, K. P., Weis, U., Stoll, B., Kuzmin, D., Yang, Q., Raczek, I., Jacob, D.E., Stracke, A., Birbaum, K., Frick, D.A., Günther, D. and Enzweiler, J., 2011. Determination of reference values for NIST SRM 610–617 glasses following ISO guidelines. *Geostandards and Geoanalytical Research*, **35**: 97–429, https://doi.org/10.1111/j.1751-908X.2011.00120.x

Kim, S.-T. and O'Neil, J.R., 1997. Equilibrium and nonequilibrium oxygen isotope effects in synthetic carbonates. *Geochimica et Cosmochimica Acta*, **61**: 3461-3475. https://doi.org/10.1016/S0016-7037(97)00169-5

Köhler, J., Konnerup-Madsen, J. and Markl, G., 2008. Fluid geochemistry in the Ivigtut cryolite deposit, South Greenland: *Lithos*, **103**: 369-392. https://doi.org/10.1016/j.lithos.2007.10.005

Ladenburger, S., Walter, B.F., Marks, M.A. and Markl, G., 2020. Combining ion chromatography and total reflection X-ray fluorescence for detection of major, minor and trace elements in quartz-hosted fluid inclusions. *Journal of Analytical Chemistry*, **75**: 1477–1485. https://doi.org/10.1134/S106193482011009X

Littke, R., Büker, C., Hertle, M., Karg, H., Stroetmann-Heinen, V. and Oncken, O., 2000. Heat flow evolution, subsidence and erosion in the Rheno-Hercynian orogenic wedge of central Europe. In W. Franke, V. Haak, O. Oncken, & D. Tanner (eds.), Orogenic processes: Quantification and modelling in the Variscan Belt. *Special Publication – Geological Society of London*, **179**: 231–255. https://doi.org/10.1144/GSL.SP.2000.179.01.15

Murray, S.T., Arienzo, M.M. and Swart, P.K., 2016. Determining the Δ47 acid fractionation in dolomites. *Geochimica et Cosmochimica Acta,* **174**: 42–53. https://doi.org/10.1016/j.gca.2015.10.029

Merritt, D.A. and Hayes, J.M, 1994. Factors controlling precision and accuracy in isotope-ratio-monitoring mass spectrometry. *Anal. Chem.*, **66**(14): 2336-2347. https://doi.org/10.1021/ac00086a020

Paton, C., Hellstrom, J., Paul, B., Woodhead, J. and Hergt, J., 2011. Iolite: Freeware for the visualization and processing of mass spectrometric data. *J. Anal. At. Spectrom.*, **26**: 2508-2518. https://doi.org/10.1039/C1JA10172B

Pearce, N.J.G., Perkins, W.T., Westgate, J.A., Gorton, M.P., Jackson, S.E., Neal, C.R. and Chenery, S.P., 1997. A compilation of new and published major and trace element data for NIST SRM 610 and NIST SRM 612 glass reference materials. *Geostandards Newsletter: The Journal of Geostandards and Geoanalysis*, **21**: 115–144. https://doi.org/10.1111/j.1751-908X.1997.tb00538.x

Pederson, C., Mueller, M., Lippert, K., Igbokwe, O.A., Riechelmann, S., Lersch, S., Benger, P., Verdecchia, A., Immenhauser, A., 2021. Impact of a regional fault zone on the properties of a deep geothermal carbonate reservoir unit (Devonian of NRW). *Z. Dt. Ges. Geowiss. (J. Appl. Reg. Geol.)*, **172**: 339–364. https://doi.org/10.1127/zdgg/2021/0281

Sharma, T. and Clayton, R.N., 1965. Measurement of O^{18}/O^{16} ratios of total oxygen of carbonates: *Geochimica et Cosmochimica Acta*, **29**: 1347–1353. https://doi.org/10.1016/0016-7037(65)90011-6

Shepherd, T.J., Rankin A.H. and Alderton, D.H.M., 1985. *A Practical Guide to Fluid Inclusion Studies.* Glasgow and London (Blackie), xi, 239 p.

Sibley, D.F. and Gregg, J.M., 1987. Classification of Dolomite Rock Texture. *Journal of Sedimentary Petrology*, **57**: 967-975. https://doi.org/10.1306/212F8CBA-2B24-11D7-8648000102C1865D

Steele-MacInnis, M., Bodnar, R.J. and Naden, J., 2011. Numerical model to determine the composition of H_2O–$NaCl$–$CaCl_2$ fluid inclusions based on microthermometric and microanalytical data. *Geochimica et Cosmochimica Acta*, **75**: 21–40. https://doi.org/10.1016/j.gca.2010.10.002

Swart, P.K., Murray, S.T., Staudigel, P.T. and Hodell, D.A., 2019. Oxygen isotopic exchange between CO_2 and phosphoric acid: Implications for the measurement of clumped isotopes in carbonates. *Geochemistry, Geophysics, Geosystems*, **20**: 3730-3750. https://doi.org/10.1029/2019GC008209

Walter, B.F., Immenhauser, A., Geske, A. and Markl, G., 2015. Exploration of hydrothermal carbonate magnesium isotope signatures as tracers for continental fluid aquifers, Schwarzwald mining district, SW Germany. *Chemical Geology*, **400**: 87–105. https://doi.org/10.1016/j.chemgeo.2015.02.009

Walter, B.F., Kortenbruck, P., Scharrer, M., Zeitvogel, C., Wälle, M., Mertz-Kraus, R. and Markl, G., 2019. Chemical evolution of ore-forming brines–Basement leaching, metal provenance, and the redox link between barren and ore-bearing hydrothermal veins. A case study from the Schwarzwald mining district in SW-Germany. *Chemical Geology*, **506**: 126-148. https://doi.org/10.1016/j.chemgeo.2018.12.038

Figure captions:

Fig. S1.1. Additional transmitted light and corresponding cathodoluminescence images of the Massenkalk limestone and Variscan thrust-related carbonates in the Steltenberg quarry. (A, B) Bright red luminescent MK limestone clast including deep-burial related idiomorphic authigenic quartz crystals grown in the matrix. These clasts belong to Breccia 1 and are "floating" in Dol 2B saddle dolomite cement. (C, D) Patchy luminescent Dol 2B saddle dolomite cement surrounds a Dedol 1 clast. Note the pore-filling meteoric cement LMC 9. (E, F) Partially recrystallized dark red luminescent dolo-grainstone Dol 1. Volumetrically, about 40% of the bulk rock now consists of bright red luminescent Dol 2. (G, H) Where Variscan thrust-related dolostones were affected by the Post-Variscan fault zone, Variscan dolomite cement phases were overgrown by Dol 3 cements. A clear genetic separation from the paragenetically older bright red luminescent dolomite cements is shown by dark red luminescence of Dol 3A.

Fig. S1.2. Additional transmitted light and corresponding cathodoluminescence images of the Post-Variscan fault zone related carbonates in the Steltenberg quarry. (A, B) Intense dark to pale bright blue zonation in hypidiomorphic Qz 2 cement. (C, D) Patchy dark red to orange luminescent iron-rich dedolomite (Dedol 2) overgrown by green and blue-luminescent Qz 1 and Qz 2. (E, F) Dedolomitized patchy luminescent saddle dolomite (Dol 3B) overgrown by calcite cements LMC 6 (zoned) and orange patchy luminescent LMC 7. (G, H) Pervasive overgrowth (LMC 4A) along a grain boundary in non-luminescent LMC 2. Note how cleavage planes and microfractures were also used as fluid pathways.

Fig. S1.3. Additional transmitted light and corresponding cathodoluminescence images of the Post-Variscan fault zone related carbonates in the Steltenberg quarry. (A, B) Green and dark blue luminescent Qz 3 from a quartz gangue. Note the dark centers in idiomorphic crystals. (C, D) Calcite vein (LMC 4A or 5B) in quartz overgrown by hematite crystals. (E, F) A spear-shaped Dol 3B saddle dolomite crystal overgrown by intensely non-luminescent to yellow zoned LMC 4. (G, H) Intrinsic blue luminescent LMC 9 including thin orange-yellow zonation. Note the precipitation of iron oxides in micro-karstified spots.

Fig. S1.4. Additional transmitted light and corresponding cathodoluminescence images of the Post-Variscan fault zone related carbonates in the Steltenberg quarry. (A, B) Sulphide overgrowth of patchy luminescent dedolomite (Dedol 2) and bright green luminescent Qz 1. (C, D)Partial overgrowth of orange luminescent radial LMC 5A crystals by pale yellow LMC 5B along grain boundaries. Note the partial overgrowth by LMC 9. (E, F) Dol tooth-shaped LMC 7 crystal overgrown by a thin layer of iron oxides and non-luminescent LMC 9. Note the zonation transition from bright orange-yellow patchy luminescent inclusion-rich LMC 7A to bright red zoned inclusion-lean LMC 7B. (G, H) Botryoidal-shaped LMC 10 crystals build a crust on top of karstified MK limestone and Post-Variscan fault zone precipitates. Note the magenta-to-orange-yellow luminescent transition towards the aggregate´s center.

Fig. S1.5. Additional U-Pb plots for phases Dol 2B saddle dolomite, hypogene karst filling LMC 2, LMC 4A, LMC 5A, and LMC 5B.

Figures:

Fig. S1.1.
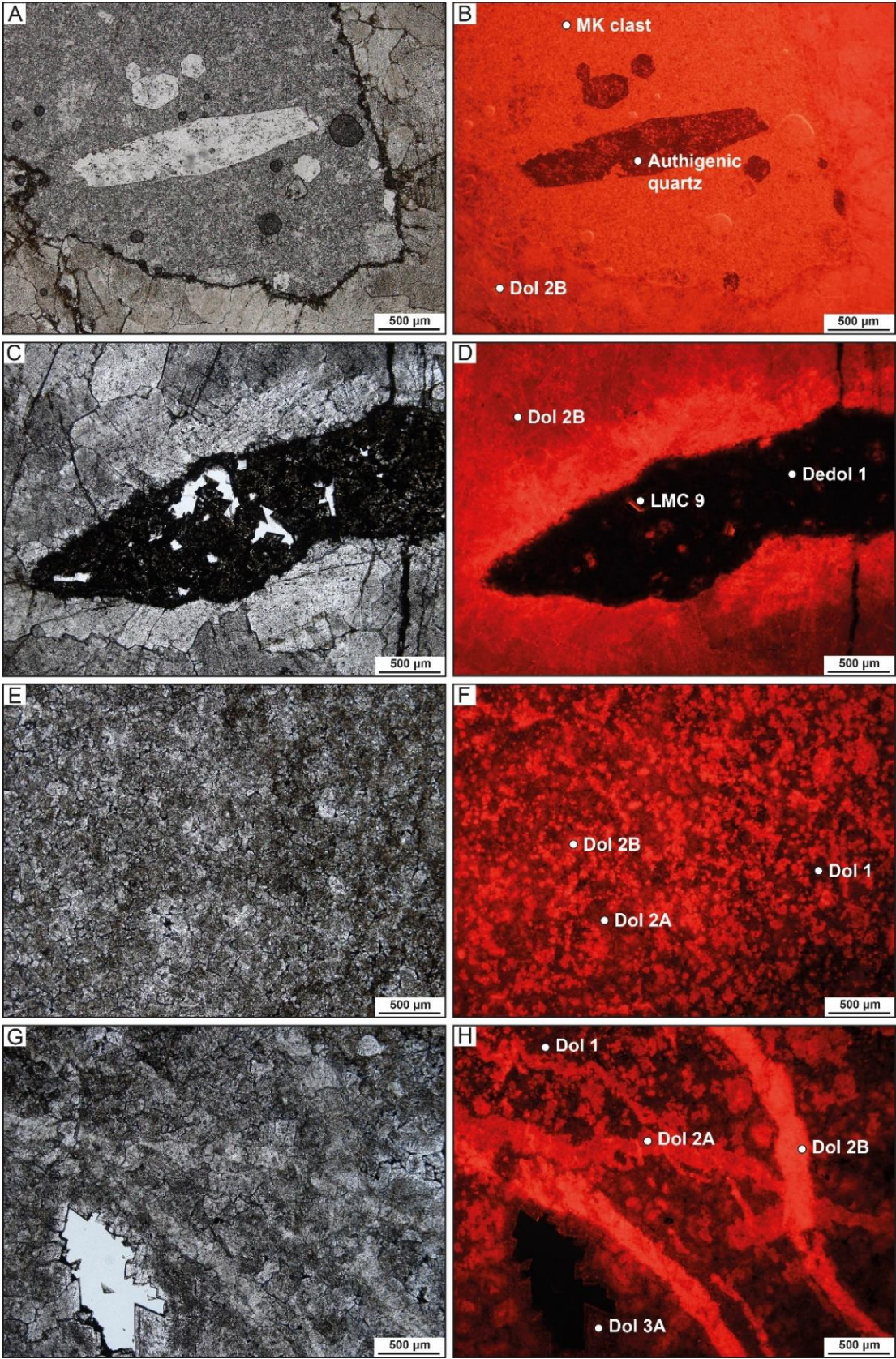
Fig. S1.2.
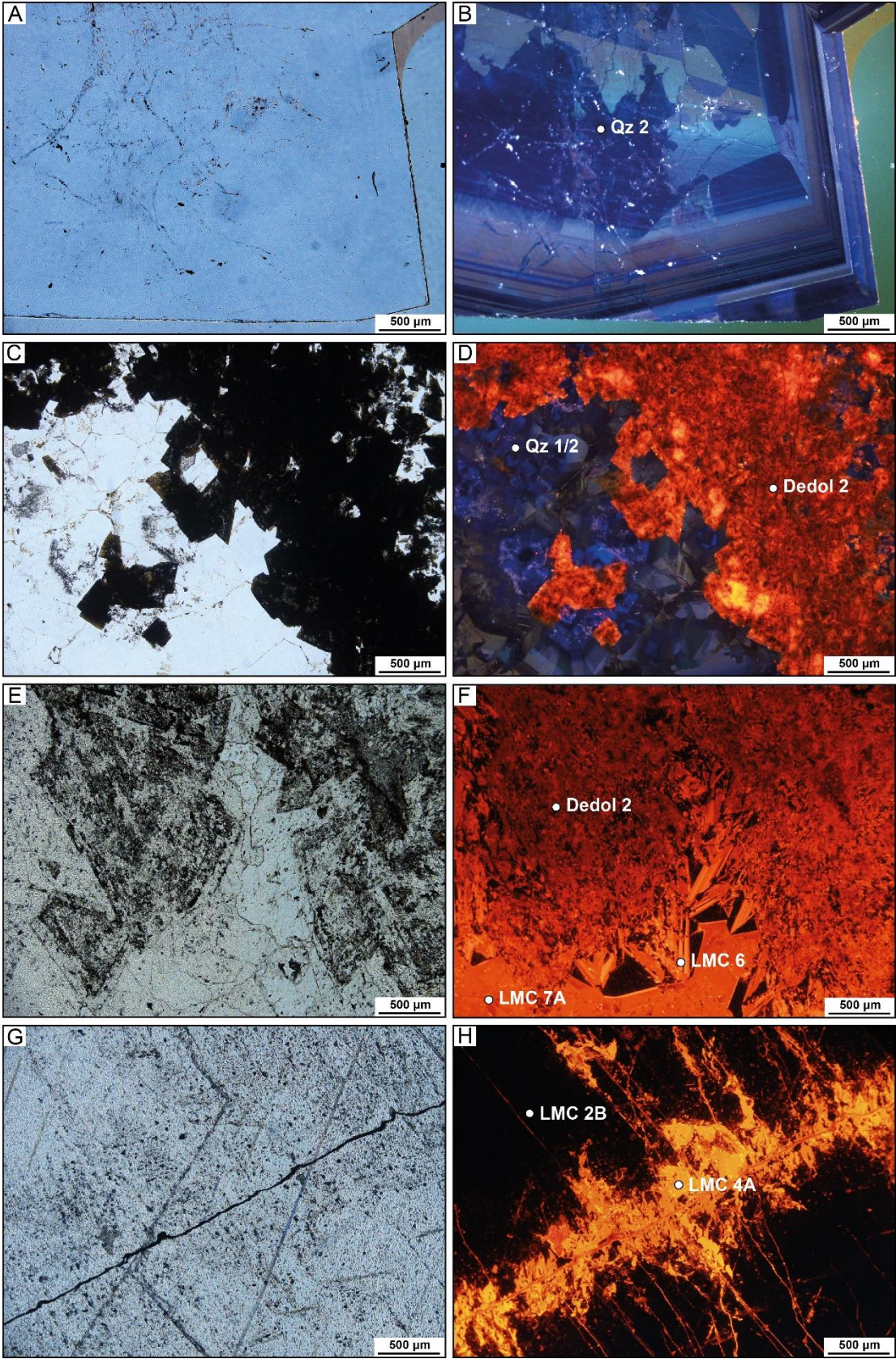
Fig. S1.3.
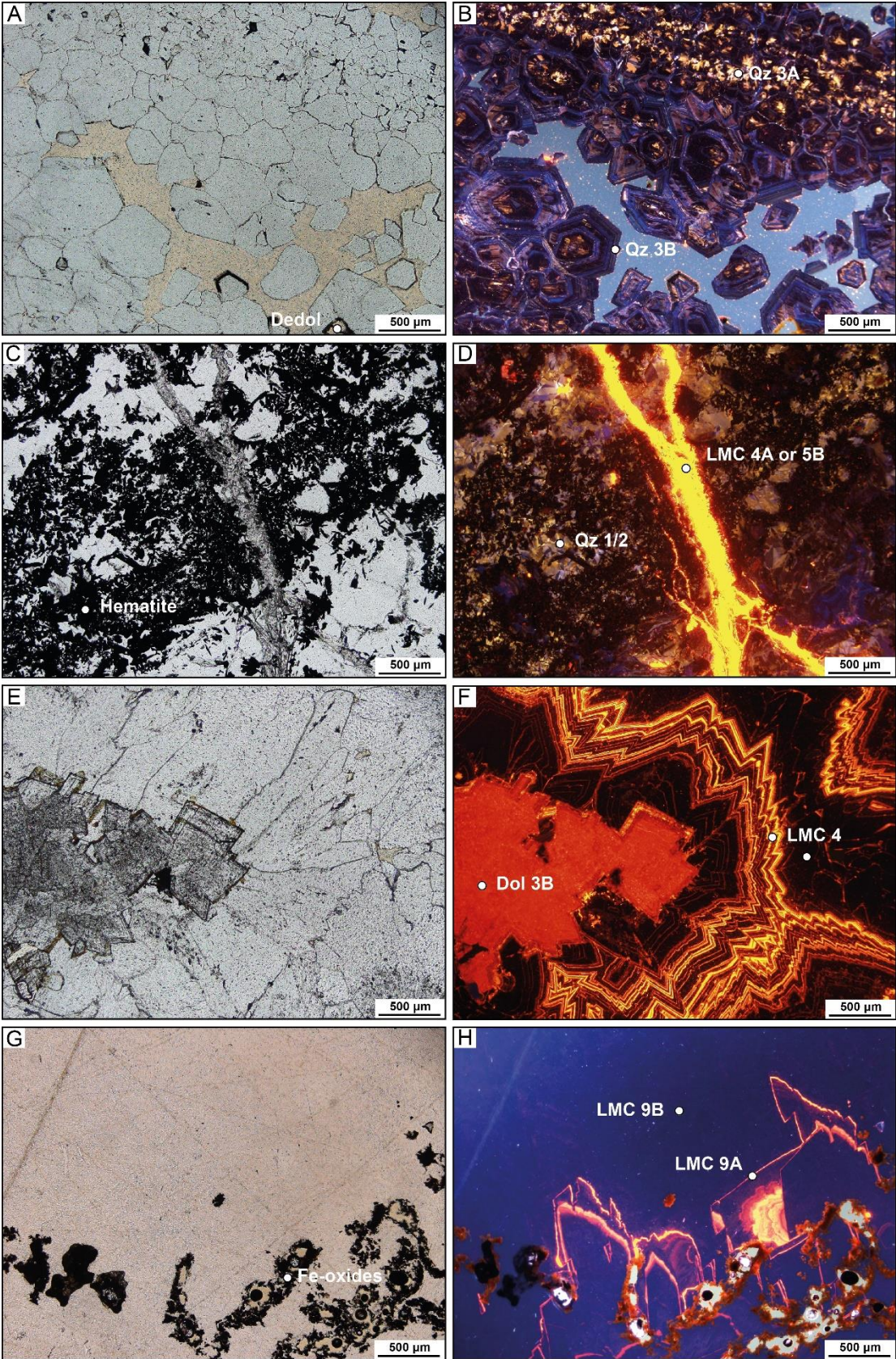
Fig. S1.4.
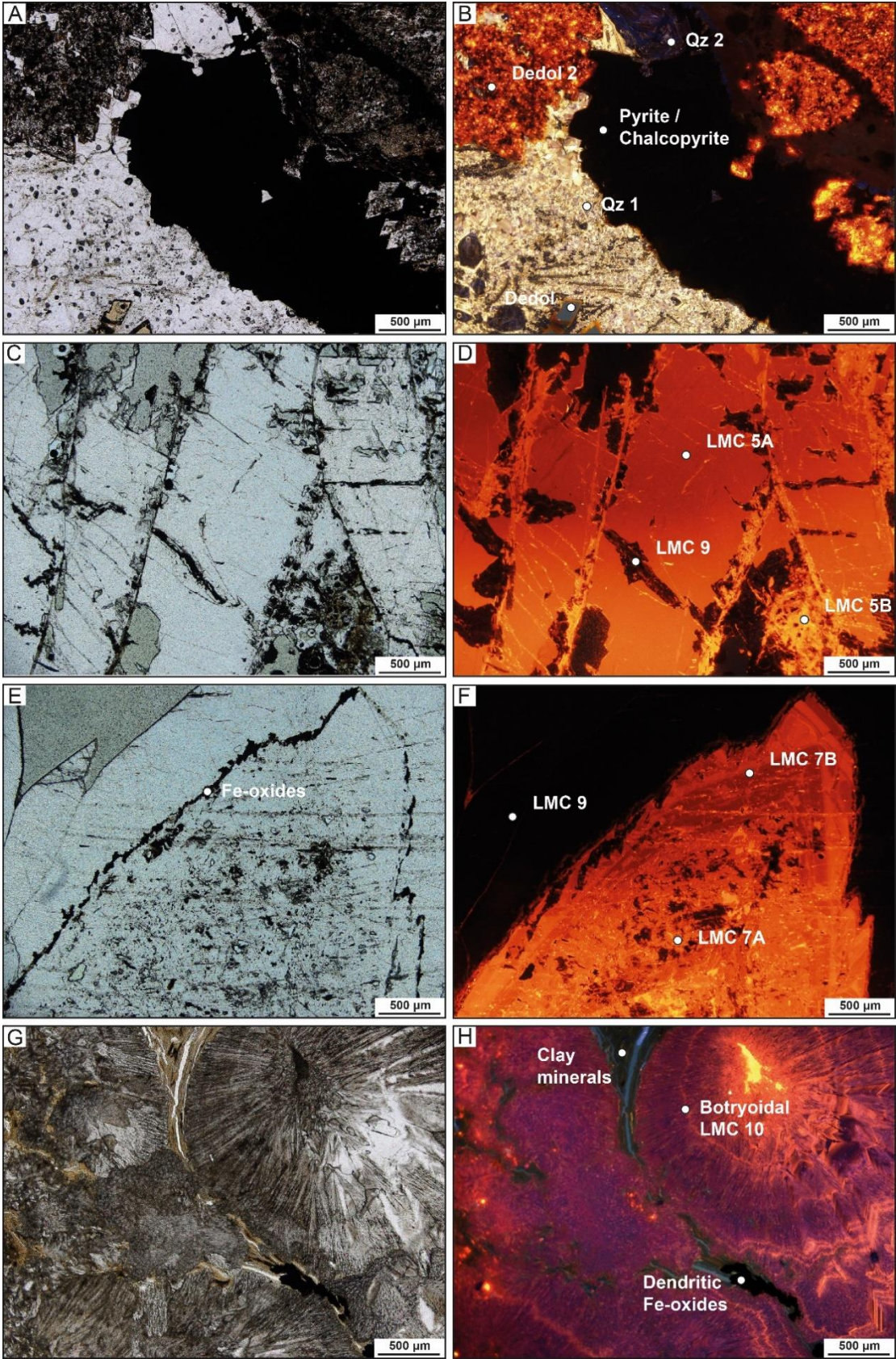
Fig. S1.5.
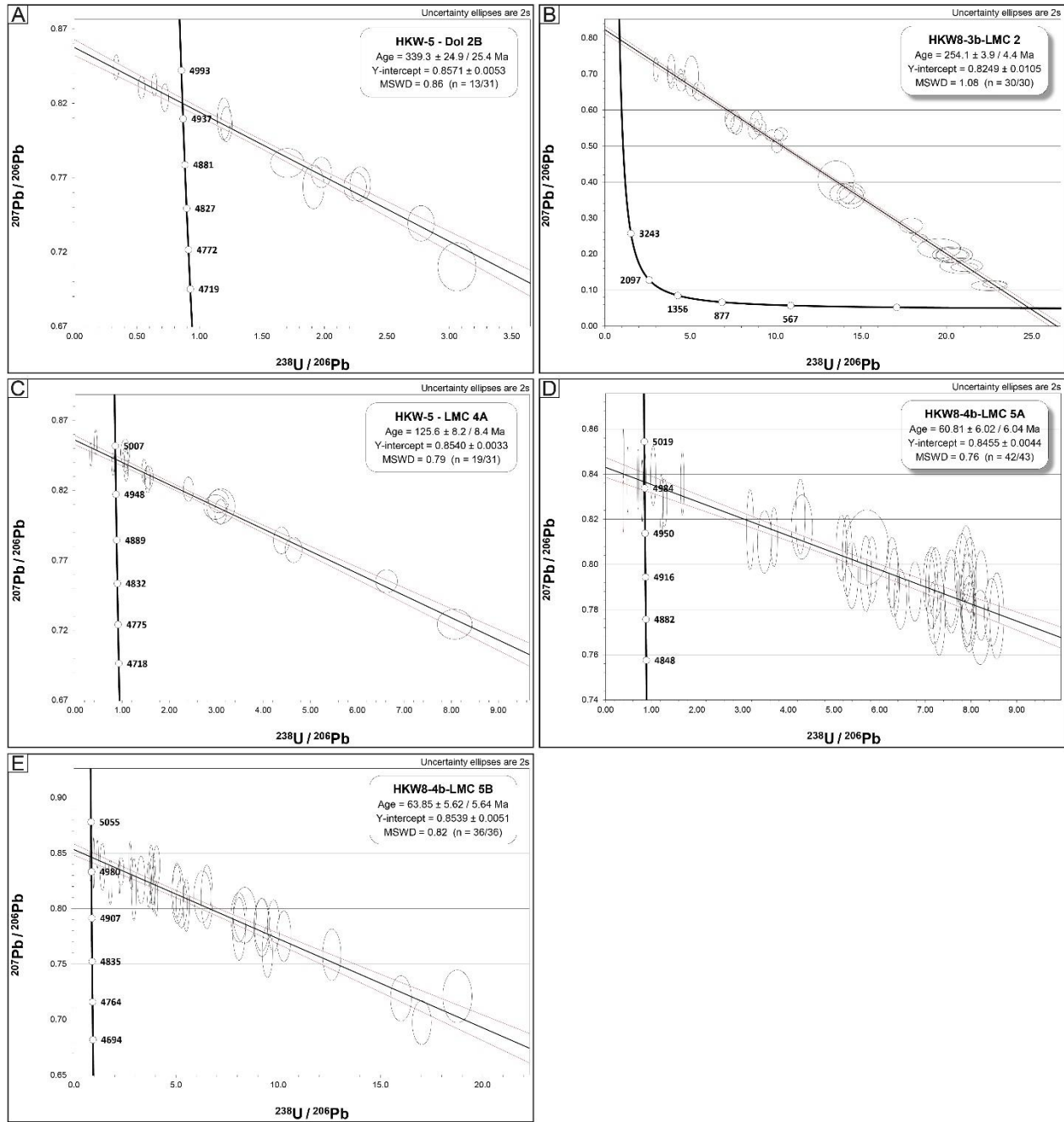
Tables:

Table S1.1. Measured strike and dip values for veins, slickensides and stretching lineations in Steltenberg Quarry.

Outcrop	Description	Level	Strike	Dip	Comment
1	Slickenside	7	10	70	
1	Slickenside	7	15	60	dextral shear
1	Slickenside	7	13	65	
1	Stretching lineation	7	304	8	
1	Stretching lineation	7	290	5	
1	Slickenside	7	12	45	
2	Brecciated calcite vein	7	268	85	
2	Brecciated calcite vein	7	258	75	
3	Calcite vein	7	258	70	Conjugated set
3	Calcite vein	7	72	68	Conjugated set
3	Calcite vein	7	74	60	Conjugated set
4	Calcite vein	7	170	60	
5	Calcite vein	7	170	70	banded
5	Calcite vein	7	165	70	banded
6	Slickenside	7	170	80	dextral shear
6	Slickenside	7	325	60	dextral shear
7	Calcite vein	7	128	65	
7	Calcite vein	7	80	45	Conjugated set
7	Calcite vein	7	84	30	Conjugated set
7	Calcite vein	7	78	25	Conjugated set
7	Calcite vein	7	210	75	red calcite cutting vein above
8	Slickenside	7	340	65	sinistral shear
8	Slickenside	7	335	60	sinistral shear
9	Slickenside	7	350	60	dextral shear
9	Stretching lineation	7	285	45	
9	Calcite and dolomite veins	7	225	85	Veins cut slickenside above
9	Calcite and dolomite veins	7	228	90	
10	Calcite vein	7	235	90	
10	Calcite vein	7	65	40	Cutting the vein above
11	GHS Calcite vein	7	243	85	
11	GHS Calcite vein	7	232	85	
12	Slickenside	7	340	45	dextral shear
12	Slickenside	7	334	55	dextral shear
12	Stretching lineation	7	30	40	
13	Ennepe Thrust	6	340	45	
13	Ennepe Thrust	6	220	85	
13	Ennepe Thrust	6	295	65	
13	Calcite vein	6	230	85	Cuts Ennepe Thrust
13	Calcite vein	6	42	85	Conjugated set
13	Calcite vein	6	350	55	Conjugated set
13	Calcite vein	6	10	85	Conjugated set
14	Slickenside	6	342	55	
14	Slickenside (old)	6	320	50	Ennepe Thrust
14	Slickenside (young) overprinting old	6	185	30	Großholtshausener Sprung
15	Saddle dolomite vein	5	8	60	Saddle dol vein from Fig. 3
16	Calcite vein	5	114	90	
16	Calcite vein	5	72	85	
16	Calcite vein	5	78	80	

Table S1.2a. Carbon, oxygen, and $^{87}Sr/^{86}Sr$ isotopic composition as well as major and trace element contents of dolomite and calcite phases from Steltenberg Quarry. Oldest phases at the top, youngest phases at the bottom. Gaps in data are indicative of variations in sampling density.

Sample	$\delta^{13}C^{PDB}$ [‰]	$\delta^{18}O^{PDB}$ [‰]	Paragenetic phase	$^{87}Sr/^{86}Sr$	± 2 σ mean	Ca	Mg	Sr	Fe	Mn
MK-S-2.1	3.2	-6.4	MK bulk matrix			272030	12220	808.0	10930.0	257.0
MK-S-2.2	3.1	-6.9	MK bulk matrix			287200	8031	900.4	7511.0	259.0
MK-S-2.3	3.1	-6.6	MK bulk matrix			280630	7724	917.2	7885.0	237.0
HKW5-MK-S-2-Ch1	2.97	-6.51	MK bulk matrix	0.708420	0.000005	257080	9007	513.6	8218.0	242.0
HKW8-8.1	2.63	-5.32	MK bulk no fossils			391350	4008	269.3	226.9	62.6
HKW8-8.2	2.42	-5.19	MK bulk no fossils	0.708027	0.000005	393100	4269	264.2	251.7	80.2
HKW8-8.3	2.82	-5.47	MK bulk no fossils			392600	3537	251.5	186.6	57.2
HKW-5-63.9	2.43	-9.49	MK bulk no fossils			389280	11340	174.5	956.9	820.0
HKW-5-63.10	2.51	-9.53	MK bulk no fossils			390260	8616	175.1	774.6	776.0
HKW-5-63.11	2.51	-9.95	MK bulk no fossils	0.708879	0.000005	396190	5109	178.5	622.1	705.0
HKW-5-63.13	2.96	-7.11	Brachiopod shell	0.707915	0.000005	399670	2867	443.3	235.3	405.0
HKW-5-63.14	2.75	-7.20	Brachiopod shell			398000	4455	488.2	364.6	404.0
HKW-5-63.15	2.83	-7.72	Brachiopod shell			403170	3126	415.1	292.5	491.0
MKHD-W-6.1	3.4	-9.4	Dol 1A			211740	124000	27.1	738.7	923.0
MKHD-W-6.2	3.5	-9.2	Dol 1A			213940	123500	25.8	425.5	786.0
MKHD-W-6.3	3.4	-9.5	Dol 1A	0.709655	0.000005	212400	122900	24.1	419.5	853.0
MKHD-W-6-3.1	3.6	-9.1	Dol 1A			217050	125500	30.6	590.4	815.0
MKHD-W-6-3.2	3.6	-9.0	Dol 1A			215590	124600	26.8	839.0	1200.0
MKHD-W-6-3.3	3.6	-8.9	Dol 1A			215160	125400	23.6	759.3	1120.0
HKW5-61-Ch2	3.73	-5.10	Dol 1A	0.709707	0.000005	205230	105400	64.9	9551.0	1320.0
HKW-5-61.2	3.88	-5.58	Dol 1A			212050	110800	89.3	9345.0	1600.0
HKW-5-61.3	3.86	-5.38	Dol 1A			214270	109400	98.7	8020.0	1510.0
HKW-5-61.4	3.81	-5.17	Dol 1A			212820	106500	117.5	8148.0	1160.0
HKW-5-61.5	3.62	-5.82	Dol 1A			212590	110500	58.8	7097.0	1570.0
HKW-5-61.10	3.62	-6.04	Dol 1A			214890	110700	61.3	7387.0	1370.0
HKW-5-61.11	3.73	-6.16	Dol 1A			213320	110300	58.0	7335.0	1460.0
HKW-5-61.12	3.62	-6.09	Dol 1A			221910	109900	83.5	5367.0	854.0
HKW-5-61.13	3.72	-5.03	Dol 1A			209590	105300	108.1	7391.0	662.0
HKW-5-61.14	3.81	-4.62	Dol 1A			202690	101400	101.6	6958.0	626.0
HKW-5-61.15	3.81	-4.52	Dol 1A	0.710021	0.000005	204630	103600	99.3	7414.0	610.0
HKW-5-61.19	3.57	-6.21	Dol 1A			220470	113400	60.3	6863.0	1380.0
HKW-5-61.20	3.63	-5.92	Dol 1A			218770	109900	72.8	8598.0	1550.0
HKW5-61-Ch1	3.54	-9.40	Dol 1B	0.708870	0.000005	223970	121900	74.8	912.8	144.0
HKW-5-61.6	3.64	-8.74	Dol 1B			223980	121000	64.1	994.8	123.0
HKW-5-61.7	3.54	-9.40	Dol 1B			224950	119700	79.4	1236.0	149.0
HKW-5-61.8	3.60	-8.68	Dol 1B			230110	119300	84.3	1180.0	139.0
HKW-5-61.9	3.67	-8.24	Dol 1B			225450	119500	72.4	1069.0	203.0
HKW-5-61.16	3.55	-10.14	Dol 1B			223610	124000	54.4	1358.0	154.0
HKW-5-61.17	3.47	-9.63	Dol 1B			230530	118500	83.4	996.7	184.0
HKW-5-61.18	3.69	-9.21	Dol 1B			224800	123600	56.2	1418.0	139.0
MKHD-W-5.1	3.8	-7.1	Dol 2A			215590	119700	23.1	7885.0	2140.0
MKHD-W-5.2	3.8	-7.0	Dol 2A	0.709786	0.000005	215290	119000	24.0	8107.0	2240.0
MKHD-W-5.3	3.8	-7.3	Dol 2A			216110	119800	24.3	6907.0	1890.0
MKHD-W-6-3.4	3.4	-7.8	Dol 2A			216560	121200	43.4	3945.0	1460.0
MKHD-W-6-3.5	3.4	-8.0	Dol 2A			213610	119800	39.5	4105.0	1540.0
MKHD-W-6-3.6	3.3	-7.8	Dol 2A			215960	121700	42.6	4552.0	1660.0
HKW5-63-Ch1	3.6	-7.5	Dol 2A	0.709236	0.000005	220210	120400	28.8	5017.0	1670.0
HKW-5-63.3	2.86	-8.21	Dol 2A			225000	125500	48.7	285.7	348.0
HKW-5-63.4	1.83	-9.02	Dol 2A			240390	111300	66.4	1153.0	1150.0
HKW-5-63.5	1.37	-8.41	Dol 2A			253010	102800	66.2	1285.0	942.0
HKW-5-63.16	3.48	-7.34	Dol 2A			225690	120200	38.9	5567.0	1950.0
HKW-5-63.18	3.06	-6.65	Dol 2A			226910	115100	30.9	7489.0	2410.0
HKW-5-63.20	3.24	-6.64	Dol 2A	0.709403	0.000005	228760	118200	32.4	7391.0	2410.0
MKHD-W-6-2.10	3.6	-9.5	Dol 2B			213600	123600	30.0	852.9	558.0
MKHD-W-6-2.11	3.4	-9.5	Dol 2B	0.709524	0.000005	213520	126900	37.6	691.3	563.0
MKHD-W-6-2.12	3.5	-9.3	Dol 2B			215970	125100	32.6	827.9	769.0
HKW5-63-Ch2	3.10	-9.14	Dol 2B	0.708861	0.000005	219980	124700	34.0	140.2	232.0
HKW-5-63.1	3.31	-8.86	Dol 2B			224310	125500	36.1	315.3	827.0

Table S1.2b. Carbon, oxygen, and ^{87}Sr/^{86}Sr isotopic composition as well as major and trace element contents of dolomite and calcite phases from Steltenberg Quarry. Oldest phases at the top, youngest phases at the bottom. Gaps in data are indicative of variations in sampling density.

Sample	δ^{13}C^{PDB} [‰]	δ^{18}O^{PDB} [‰]	Paragenetic phase	^{87}Sr/^{86}Sr	±2 σ$_{mean}$	Ca	Mg	Sr	Fe	Mn
HKW-5-63.2	3.28	-8.74	Dol 2B			224630	125700	39.8	449.5	957.0
HKW-5-63.6	2.95	-9.24	Dol 2B			222660	127300	40.1	261.7	231.0
HKW-5-63.7	2.90	-9.39	Dol 2B			223790	126900	45.3	189.9	263.0
HKW-5-63.8	3.13	-9.80	Dol 2B			223840	127900	51.4	305.3	282.0
HKW-5-63.12	2.97	-5.77	Dol 2B			226780	116800	20.9	10550.0	2960.0
HKW-5-63.17	2.17	-6.00	Dol 2B			271820	52770	24.7	6208.0	2220.0
HKW-5-63.19	2.85	-5.39	Dol 2B			230640	113000	19.6	10990.0	3240.0
MKHD-W-6.4	0.5	-7.3	Dedol 1			267660	91880	37.0	1539.0	1690.0
MKHD-W-6.5	-2.5	-5.8	Dedol 1			308130	59190	32.9	2537.0	2180.0
MKHD-W-6.6	-3.3	-5.5	Dedol 1	0.709334	0.000004	326230	50340	29.9	2672.0	2110.0
MKHD-S-1.2	1.7	-13.9	LMC 1			400820	2080	167.5	77.2	286.0
MKHD-S-1.3	1.9	-13.7	LMC 1	0.708757	0.000005	399850	1757	92.8	175.4	387.0
MKHD-W-5.4	2.2	-8.6	LMC 1			400890	2541	395.1	590.2	310.0
MKHD-W-5.5	2.0	-8.4	LMC 1			380440	3462	363.5	690.4	328.0
MKHD-W-5.6	1.7	-11.3	LMC 1			397750	3447	596.2	713.3	391.0
MKHD-W-6-2.7	1.8	-11.9	LMC 1			402060	1199	28.1	54.5	553.0
MKHD-W-6-2.8	2.0	-11.7	LMC 1			396650	2046	38.4	69.8	766.0
MKHD-W-6-2.9	1.3	-11.2	LMC 1			391480	3742	40.2	121.7	578.0
HKW5-MKHD-W-6-Ch1	1.93	-11.69	LMC 1	0.709314	0.000005	396320	1283	48.6	51.9	829.0
MKHD-E-7.1	3.6	-7.2	Dol 3A			206890	119600	19.8	9027.0	2160.0
MKHD-E-7.2	3.5	-7.2	Dol 3A			204500	114000	20.5	8635.0	2180.0
MKHD-E-7.3	3.5	-7.1	Dol 3A			196610	110800	20.1	7774.0	1820.0
HKW5-MKHD-E-7-Ch1	3.81	-6.98	Dol 3A	0.708565	0.000005	209750	118400	17.9	8932.0	2210.0
MKHD-E-7.4	3.68	-7.20	Dol 3A	0.708574	0.000005	205270	117600	19.1	8644.0	2130.0
MKHD-E-7.6	3.65	-7.23	Dol 3A			207510	119600	18.1	8257.0	2120.0
HKW8-Dol3A.1	3.18	-6.86	Dol3A			208800	114900	21.3	14830.0	3480.0
HKW8-Dol3A.2	3.35	-6.94	Dol3A			212790	119700	24.5	15260.0	3480.0
HKW8-Dol3A.3	3.26	-7.15	Dol3A			210720	117800	23.6	14400.0	3600.0
HKW8-Dol3A.4	3.38	-6.91	Dol3A			210840	120400	22.7	13970.0	3080.0
HD-S-3.1.1	0.5	-3.4	Dol 3B	0.709047	0.000005	215720	125200	20.4	5831.0	2980.0
HD-S-3.1.2	0.4	-3.7	Dol 3B			215730	124800	17.1	5855.0	2690.0
HD-S-3.1.3	0.6	-4.3	Dol 3B			214010	122500	39.3	6809.0	2860.0
HKW5-HD-S-3.1-Ch1	0.5	-4.4	Dol 3B	0.709064	0.000004	212750	122700	14.0	7293.0	3120.0
HKW8-1-Ch1	2.9	-6.5	Dol 3B fault core	0.708626	0.000005	213000	119900	14.2	11760.0	2580.0
HKW8-1.1	2.65	-6.45	Dol 3B			213810	121900	14.4	10850.0	2470.0
HKW8-1.2	2.75	-6.42	Dol 3B			212580	121100	13.2	10670.0	2370.0
HKW8-1.3	3.02	-6.58	Dol 3B			211350	119500	12.2	12510.0	2600.0
HKW-5-64.1	-0.54	-6.05	Dol 3B			173690	62120	14.6	6502.0	2350.0
HKW-5-64.2	-0.90	-5.76	Dol 3B			273670	84810	20.0	10020.0	3480.0
HKW-5-64.3	-1.24	-5.78	Dol 3B			271110	83280	20.1	9765.0	3400.0
HKW-5-64.12	0.39	-5.66	Dol 3B			242610	100100	20.1	8077.0	2800.0
HKW-5-64.13	0.19	-5.72	Dol 3B			240940	99180	20.2	7955.0	2820.0
HKW-5-64.20	-1.28	-4.54	Dol 3B			256570	85720	23.6	7585.0	3090.0
HKW7-CZ3.1	4.60	-5.64	Dol 3B			219880	118100	12.1	17690.0	4050.0
HKW7-CZ3.2	4.21	-5.61	Dol 3B			225370	112500	17.5	17410.0	4060.0
HKW8-Dol3B.1	2.88	-7.02	Dol3B			199590	113200	24.4	11520.0	2500.0
HKW8-Dol3B.2	3.00	-6.82	Dol3B			186780	107300	19.5	11450.0	2540.0
HKW8-Dol3B.3	3.06	-6.73	Dol3B			211370	121100	23.0	13190.0	2780.0
HKW8-Dol3B.4	2.88	-6.85	Dol3B			211870	120300	23.1	13720.0	2990.0
HKW7-GH1.1	-2.08	-4.50	Lam 1 Dol cc	0.709028	0.000005	212960	125100	14.3	6269.0	2630.0
HKW7-GH1.2	-2.19	-4.18	Lam 1 Dol cc			209210	122500	18.2	5080.0	2530.0
HKW7-GH1.3	-2.86	-2.13	Lam 1 Dol3B			211820	123500	19.8	3409.0	2400.0
HKW7-GH1.4	-2.76	-0.41	Lam 1 clayey dolopackstone	0.714721	0.000006	142360	83270	21.7	2189.0	1620.0
HKW7-GH1.5	-3.04	-0.81	Lam 1 clayey dolopackstone			128490	73880	18.1	1553.0	1480.0
HKW7-GH1.6	-2.86	-1.96	Lam 1 clayey dolopackstone			131980	75730	19.1	2500.0	1500.0
HKW8-3-Ch1	-2.92	-5.77	LMC 2	0.711326	0.000005	399310	2245	346.7	28.5	24.5
HKW8-3.1	-3.09	-6.41	LMC 2			395340	2501	179.4	138.7	136.0
HKW8-3.2	-2.50	-6.37	LMC 2			395410	2283	200.9	186.7	211.0

Table S1.2c. Carbon, oxygen, and [87]Sr/[86]Sr isotopic composition as well as major and trace element contents of dolomite and calcite phases from Steltenberg Quarry. Oldest phases at the top, youngest phases at the bottom. Gaps in data are indicative of variations in sampling density.

Sample	$\delta^{13}C^{PDB}$ [‰]	$\delta^{18}O^{PDB}$ [‰]	Paragenetic phase	$^{87}Sr/^{86}Sr$ ± 2 σ_{mean}	Ca	Mg	Sr	Fe	Mn
HD-S-3.0.1	-7.0	-6.1	Dedol 2			362850	8653	17.3	2424.0	1680.0
HD-S-3.0.2	-7.4	-6.0	Dedol 2			372740	7859	17.9	2408.0	1640.0
HD-S-3.0.3	-7.4	-6.0	Dedol 2	0.709761 0.000005	372650	7512	17.2	2379.0	1560.0
HKW8-2-Ch1	-2.78	-5.36	Dedol 2	0.709934 0.000006	339840	10940	58.6	2342.0	2030.0
HKW8-2.1	-4.40	-5.49	Dedol 2			364510	13270	48.7	3509.0	2330.0
HKW8-2.2	-1.87	-5.56	Dedol 2			352380	20690	58.7	3200.0	3160.0
HKW-5-64.4	-5.91	-5.97	Dedol 2			339190	26680	18.2	7190.0	3800.0
HKW-5-64.5	-6.36	-4.56	Dedol 2			361630	15290	18.3	5076.0	2900.0
HKW-5-64.6	-7.28	-5.68	Dedol 2			358660	8926	17.5	5746.0	2910.0
HKW-5-64.7	-7.01	-5.68	Dedol 2			358070	7873	15.2	5056.0	2790.0
HKW-5-64.8	-6.95	-4.40	Dedol 2			334970	24990	18.4	5292.0	3140.0
HKW-5-64.11	-2.01	-6.68	Dedol 2			273030	76850	17.0	7925.0	3320.0
HKW-5-64.18	-2.29	-6.30	Dedol 2			304600	52800	21.8	7196.0	4200.0
HKW-5-64.19	-3.24	-4.16	Dedol 2			291070	62520	19.2	6854.0	3270.0
HKW7-C1.1	2.16	-7.15	LMC 3			391470	1526	362.0	6071.0	3260.0
HKW7-C1.2	2.65	-6.95	LMC 3			385300	1565	343.9	7047.0	3550.0
HKW7-C2.1	0.86	-9.75	LMC 3	0.710094 0.000005	390330	1268	22.5	474.9	759.0
HKW7-C2.2	0.40	-6.03	LMC 3			396730	2561	285.4	358.6	157.0
HKW5-MKHD-W-6-Ch2	1.26	-8.52	LMC 4	0.712528 0.000005	399130	1632	79.4	402.3	741.0
HKW5-MKHD-W-6-Ch3	1.14	-8.68	LMC 4			399230	1421	73.0	387.7	726.0
MKHD-W-6-2.13	0.3	-6.2	LMC 5			394540	2449	213.7	127.2	178.0
MKHD-W-6-2.14	0.2	-6.2	LMC 5	0.713170 0.000005	395690	2127	224.3	112.3	200.0
MKHD-W-6-2.15	0.3	-6.2	LMC 5			399340	2103	197.0	154.5	173.0
HD-S-3.1.4	0.5	-6.9	LMC 5			392350	2007	181.6	3625.0	4180.0
HD-S-3.1.5	0.3	-6.7	LMC 5			389270	1287	171.4	3390.0	4250.0
HD-S-3.1.6	0.7	-6.7	LMC 5			381370	5634	167.5	3361.0	4400.0
HKW8-4-Ch1	1.65	-6.32	LMC 5			399120	783	186.4	3797.0	3000.0
HKW8-5-Ch1	-0.68	-6.13	LMC 5	0.711526 0.000005	399740	2083	348.9	160.6	266.0
HKW5-65.1	-0.74	-5.35	LMC 5			398820	2949	554.2	111.2	223.0
HKW5-65.2	0.40	-5.56	LMC 5			395710	2410	245.3	81.2	170.0
HKW8-4.1	1.09	-5.97	LMC 5			396050	673	195.3	3837.0	3090.0
HKW8-4.2	2.06	-6.58	LMC 5			395250	973	213.3	5158.0	3140.0
HKW8-5.1	0.41	-6.48	LMC 5			396250	3138	234.1	187.3	263.0
HKW8-5.2	0.14	-6.54	LMC 5			394870	1843	250.9	202.8	368.0
HKW8-1-Ch2	1.41	-6.14	LMC 6	0.709306 0.000005	399260	589	104.8	1824.0	1550.0
HKW8-1.4	-0.12	-5.73	LMC 6			393540	2011	71.1	1372.0	1260.0
HKW8-1.5	1.76	-6.15	LMC 6	0.709106 0.000005	399320	363	114.1	1928.0	1680.0
HKW-5-64.14	2.08	-5.93	LMC 6			392770	850	80.3	1705.0	2310.0
HKW-5-64.15	2.00	-6.30	LMC 6			393900	348	77.3	1647.0	2240.0
HKW-5-64.16	0.37	-5.64	LMC 6			396740	1336	74.0	1402.0	1310.0
HKW-5-64.17	2.05	-6.36	LMC 6			398890	390	80.9	1718.0	2350.0
HKW7-CZ3.3	2.07	-5.27	LMC 6A	0.708658 0.000005	394090	1511	114.4	1510.0	2000.0
HKW7-CZ3.4	2.26	-5.42	LMC 6A			395910	662	101.7	1145.0	1860.0
HKW7-CZ3.5	2.23	-5.44	LMC 6A			394580	740	107.1	1217.0	1850.0
HKW7-CZ3.6	1.91	-6.14	LMC 6B	0.709035 0.000005	394880	350	118.8	1742.0	2040.0
HKW7-CZ3.7	1.90	-6.32	LMC 6B			395090	340	91.8	1657.0	1530.0
HKW7-CZ3.8	1.96	-6.18	LMC 6B			394530	350	102.2	1668.0	2020.0
HKW8-5-Ch2	1.20	-6.31	LMC 7	0.709161 0.000005	400690	379	90.9	1777.0	2940.0
HKW8-6-Ch1	2.59	-6.19	LMC 7	0.709506 0.000005	393600	944	175.0	4878.0	3370.0
HKW8-6.1	2.00	-7.45	LMC 7			393660	975	183.8	6495.0	3300.0
HKW8-6.2	2.50	-5.89	LMC 7			394750	593	151.7	3382.0	2430.0
HKW8-5.3	1.32	-6.26	LMC 7			391110	312	92.7	1812.0	3740.0
HKW8-5.4	-0.44	-6.00	LMC 7			388250	1015	162.9	2568.0	1570.0
HKW7-GH1.7	-2.88	-3.75	LMC 8 + LMC 9	0.711656 0.000005	400130	2744	64.3	1632.0	800.0
HKW7-GH1.8	-1.47	-3.42	LMC 8+ LMC 9			391160	3047	79.0	2323.0	1670.0
HKW8-5-Ch3	-3.58	-5.75	LMC 9	0.709386 0.000005	401050	2415	44.8	1088.0	567.0
HKW8-5.5	-4.09	-5.02	LMC 9			440190	2392	77.5	1486.0	617.0
HKW8-5.6	-5.27	-5.29	LMC 9			391510	2789	39.5	434.3	213.0
HKW-6-Schl 1.1.1	-5.96	-8.11	LMC 10			362360	1559	9.5	703.9	20.8
HKW-6-Schl 1.1.2	-6.11	-8.02	LMC 10			362170	1689	9.5	783.4	7.1
HKW-6-Schl 1.1.3	-5.57	-9.23	LMC 10			369270	1111	9.1	247.7	107.0
HKW-6-Schl 1.2.1	-6.10	-8.00	LMC 10			298480	2126	13.7	4158.0	450.0
HKW-6-Schl 1.2.2	-6.40	-7.51	LMC 10			276780	1847	17.9	2077.0	151.0
HKW-6-Schl 1.2.3	-6.11	-8.17	LMC 10			285780	2322	15.9	1449.0	298.0

Table S1.3. Clumped isotope data for carbonate samples from Steltenberg Quarry.

Sample	Paragenetic phase	253 plus δ^{13}C	sd	δ^{18}O	sd	Δ_{47}	T [°C]	sd	##
HKW5-MKS-2-Ch1	MK limestone	3.19	0.03	-6.06	0.10	0.47	85	41	2
HKW5-61-Ch2	Dol 1A	3.79	0.05	-6.19	0.04	0.41	124	5	2
HKW5-61-Ch1	Dol 1B	3.62	0.05	-10.22	0.19	0.35	181	13	2
HKW5-63-Ch1	Dol 2A	3.75	0.01	-8.24	0.13	0.46	90	38	2
HKW5-63-Ch2	Dol 2B	3.11	0.09	-10.14	0.42	0.38	146	21	2
HKW5-MKHD-W-6-Ch1	LMC 1	2.07	0.00	-10.92	0.09	0.32	227	17	2
HKW5-MKHD-E7-Ch1	Dol 3A	3.79	0.09	-8.02	0.28	0.40	130	23	2
HKW8-1-Ch1	Dol 3B	2.95	0.05	-7.57	0.18	0.40	133	34	3
HKW7-GH1.1	Lam 1 Dol cc	-2.41	0.01	-4.80	0.04	0.47	80	22	2
HKW7-GH1.4	Lam 1 clayey dolopackstone	-2.80	0.13	-1.96	0.36	0.43	106	14	3
HKW8-3-Ch1	LMC 2	-2.66	0.02	-5.50	0.05	0.53	48	4	2
HKW8-2-Ch1	Dedol 2	-2.68	0.18	-5.36	0.33	0.59	27	11	3
HKW8-1-Ch2	LMC 3	1.49	0.05	-5.95	0.16	0.52	57	21	2
HKW5-MKHD-W-6-Ch2	LMC 4	1.35	0.13	-8.32	0.40	0.44	102	8	2
HKW8-5-Ch1	LMC 5	-0.61	0.04	-5.87	0.03	0.47	81	30	2
HKW7-CZ3.6	LMC 6	2.01	0.30	-6.03	0.15	0.48	78	14	2
HKW8-5-Ch2	LMC 7	1.26	0.04	-5.96	0.02	0.53	50	1	2
HKW7-CZ3.3	LMC 8	2.04	0.10	-5.94	0.84	0.48	73	1	2
HKW8-5-Ch3	LMC 9	-3.33	0.1	-5.46	0.18	0.61	23	8	3

Table S1.4a. Fluid inclusion data for dolomite-, dedolomite-, calcite- and quartz phases from Steltenberg quarry. Palaeooverburden thickness was compiled from Drozdzewski and Wrede (1994) and Götte (2004).

Sample	Mineral	Host	Estimated min. overburden [m]	FIA	Inclusion type	FI	Tm (I)	Th Halite	Th Halite corr.	Th hh corr.	Density
MKHD-W4	dolomite	Dol 1A	2,000	cDol1-1-1	cluster	1	-3.2	no halite	no halite	no hh	1.03
MKHD-W4	dolomite	Dol 1A	2,000	cDol1-1-1	cluster	2	-4.8	no halite	no halite	no hh	1.04
HKW5-61-1	dolomite	Dol 1B	3,000	pDol 1B-1-1	primary	1	-19.4	no halite	no halite	no hh	1.11
HKW5-61-1	dolomite	Dol 1B	3,000	pDol 1B-1-2	primary	2	-19.5	no halite	no halite	no hh	1.12
HKW5-61-1	dolomite	Dol 1B	3,000	pDol 1B-1-3	primary	3	-20.3	no halite	no halite	no hh	1.12
HKW5-61-1	dolomite	Dol 1B	3,000	pDol 1B-1-4	primary	4	-19.4	no halite	no halite	no hh	1.11
HKW5-61-1	dolomite	Dol 1B	3,000	pDol 1B-1-5	primary	5	-22.3	no halite	no halite	no hh	1.13
HKW5-61-1	dolomite	Dol 1B	3,000	pDol 1B-1-6	primary	6	-21.1	no halite	no halite	no hh	1.11
HKW5-61-1	dolomite	Dol 1B	3,000	pDol 1B-1-7	primary	7	-20	no halite	no halite	no hh	1.12
HKW5-61-1	dolomite	Dol 1B	3,000	cDol vein 1-1-1	cluster	1	-15.4	no halite	no halite	no hh	1.08
HKW5-61-1	dolomite	Dol 1B	3,000	cDol vein 1-1-2	cluster	2	-16.3	no halite	no halite	no hh	1.09
HKW5-61-1	dolomite	Dol 1B	3,000	cDol vein 1-1-3	cluster	3	-14.9	no halite	no halite	no hh	1.08
MKHD-W4	dolomite	Dol 2A	4,000	pDol 2A-a-1	primary	1	-27.1	no halite	no halite	-23	1.14
MKHD-W4	dolomite	Dol 2A	4,000	pDol 2A-a-2	primary	2	-25.8	no halite	no halite	-22.2	1.14
MKHD-W4	dolomite	Dol 2A	4,000	pDol 2A-a-3	primary	3	-25.6	no halite	no halite	-22.6	1.13
MKHD-W4	dolomite	Dol 2A	4,000	pDol 2A-a-4	primary	4	-25.2	no halite	no halite	-21.8	1.13
MKHD-W4	dolomite	Dol 2A	4,000	pDol 2A-b-1	primary	1	-24	no halite	no halite	-28	1.13
MKHD-W4	dolomite	Dol 2A	4,000	pDol 2A-b-2	primary	2	-24.2	no halite	no halite	-27	1.13
MKHD-W4	dolomite	Dol 2A	4,000	pDol 2A-b-3	primary	3	-23.5	no halite	no halite	-27.7	1.12
MKHD-W4	dolomite	Dol 2A	4,000	pDol 2A-b-4	primary	4	-24.7	no halite	no halite	-27.4	1.13
MKHD-W-6-1	dolomite	Dol 2A	4,000	cDol2A-1-1	cluster	1	-18.4	no halite	no halite	-23.2	1.10
MKHD-W-6-1	dolomite	Dol 2A	4,000	cDol2A-1-2	cluster	2	-17.9	no halite	no halite	-23.7	1.09
MKHD-W-6-1	dolomite	Dol 2A	4,000	cDol2A-1-3	cluster	3	-19.3	no halite	no halite	-23.2	1.11
MKHD-W-6-1	dolomite	Dol 2A	4,000	cDol2A-1-4	cluster	4	-18.6	no halite	no halite	-23.8	1.11
MKHD-W-6-1	dolomite	Dol 2A	4,000	cDol2A-1-5	cluster	5	-18.9	no halite	no halite	-22.9	1.09
MKHD-W-6-1	dolomite	Dol 2A	4,000	cDol2A-1-6	cluster	6	-17.9	no halite	no halite	-23	1.10
MKHD-W4	dolomite	Dol 2A	4,000	cDol2A-1-1	cluster	1	-19.4	no halite	no halite	-23.2	1.11
MKHD-W4	dolomite	Dol 2A	4,000	cDol2A-1-2	cluster	2	-16.3	no halite	no halite	-23.8	1.09
MKHD-W4	dolomite	Dol 2A	4,000	cDol2A-1-3	cluster	3	-16.9	no halite	no halite	-23.3	1.10
MKHD-W4	dolomite	Dol 2A	4,000	pDol 2A-a-1-1	primary	1	-24.7	no halite	no halite	-26.3	1.15
MKHD-W4	dolomite	Dol 2A	4,000	pDol 2A-a-1-2	primary	2	-24.3	no halite	no halite	-25.7	1.15
MKHD-W4	dolomite	Dol 2A	4,000	pDol 2A-b-1-1	primary	1	-26.4	no halite	no halite	-25.5	1.16
MKHD-W4	dolomite	Dol 2A	4,000	pDol 2A-b-1-2	primary	2	-26.9	no halite	no halite	-25.2	1.18
MKHD-W4	dolomite	Dol 2A	4,000	pdol 2A-c-1-1	primary	1	-27.9	-27.9	-27.9	no hh	1.17
MKHD-W6-2	dolomite	Dol 2B	4,000	cDol 2B-1-1	cluster	1	-21.4	no halite	no halite	-26.4	1.12
MKHD-W6-2	dolomite	Dol 2B	4,000	cDol 2B-1-2	cluster	2	-19.8	no halite	no halite	-24.6	1.11
MKHD-W6-2	dolomite	Dol 2B	4,000	cDol 2B-1-3	cluster	3	-18.6	no halite	no halite	-26.4	1.10
MKHD-W6-2	dolomite	Dol 2B	4,000	cDol 2B-1-4	cluster	4	-18.9	no halite	no halite	-26.4	1.11
MKHD-W6-2	dolomite	Dol 2B	4,000	cDol 2B-2-1	cluster	1	-19.7	no halite	no halite	-23.5	1.12
MKHD-W6-2	dolomite	Dol 2B	4,000	cDol 2B-2-2	cluster	2	-20.5	no halite	no halite	-23.5	1.12
MKHD-W6-2	dolomite	Dol 2B	4,000	cDol 2B-2-3	cluster	3	-21	no halite	no halite	-23.5	1.12
MKHD-W6-2	dolomite	Dol 2B	4,000	cDol 2B-2-4	cluster	4	-20.8	no halite	no halite	-23.5	1.12
MKHD-W6-2	dolomite	Dol 2B	4,000	cDol 2B-2-5	cluster	5	-20	no halite	no halite	-22.9	1.12
MKHD-W6-2	dolomite	Dol 2B	4,000	cDol 2B-2-6	cluster	6	-19.3	no halite	no halite	-22.2	1.12
MKHD-W6-2	dolomite	Dol 2B	4,000	cDol 2B-3-1	cluster	1	-21	no halite	no halite	-24.6	1.12
MKHD-W6-2	dolomite	Dol 2B	4,000	cDol 2B-3-2	cluster	2	-19.8	no halite	no halite	-24.8	1.12
MKHD-W6-2	dolomite	Dol 2B	4,000	cDol 2B-3-3	cluster	3	-19.7	no halite	no halite	-25.2	1.11
MKHD-W6-2	dolomite	Dol 2B	4,000	cDol 2B-3-4	cluster	4	-19.3	no halite	no halite	-23.9	1.12
MKHD-W6-2	dolomite	Dol 2B	4,000	cDol 2B-4-1	cluster	1	-17.9	no halite	no halite	-25.6	1.11
MKHD-W6-2	dolomite	Dol 2B	4,000	cDol 2B-4-2	cluster	2	-18.4	no halite	no halite	-25.4	1.11
MKHD-W6-2	dolomite	Dol 2B	4,000	cDol 2B-4-3	cluster	3	-19.3	no halite	no halite	-24.7	1.11
MKHD-W-6-1	dolomite	Dol 2B	4,000	cDol2B-1-1	cluster	1	-21.1	no halite	no halite	-23.6	1.12
MKHD-W-6-1	dolomite	Dol 2B	4,000	cDol2B-1-2	cluster	2	-20.9	no halite	no halite	-25.4	1.11
MKHD-W-6-1	dolomite	Dol 2B	4,000	cDol2B-1-3	cluster	3	-20.7	no halite	no halite	-25.2	1.12
MKHD-W-6-1	dolomite	Dol 2B	4,000	cDol2B-1-4	cluster	4	-20.4	no halite	no halite	-23.7	1.12

Table S1.4b. Fluid inclusion data for dolomite-, dedolomite-, calcite- and quartz phases from Steltenberg quarry. Palaeooverburden thickness was compiled from Drozdzewski and Wrede (1994) and Götte (2004).

Sample	T_h uncorr.	T_h corr.	Salinity	NaCl wt.%	CaCl$_2$ wt.%	Cl ppm	Ca ppm	Na ppm	Mole Ca	Mole Na	Mole ratio Ca/(Na+Ca)	Na deficit	Ca excess
MKHD-W4	40.0	61.0	5.4	5.4	0.0	32674.2	52	21151.4		0.9	0.00	-129.2	-28.8
MKHD-W4	40.0	59.3	7.8	7.8	0.0	47221.5	75	30568.5		1.3	0.00	-186.7	-41.7
HKW5-61-1	109.0	124.4	22.0	21.9	0.1	133152.6	210	86195.3		3.7	0.00	-526.4	-117.5
HKW5-61-1	103.0	118.1	22.0	22.0	0.1	133609.5	211	86491.1		3.8	0.00	-528.2	-117.9
HKW5-61-1	99.0	114.0	22.6	22.6	0.1	137247.2	217	88845.9		3.9	0.00	-542.6	-121.1
HKW5-61-1	106.0	121.2	22.0	21.9	0.1	133152.6	210	86195.3		3.7	0.00	-526.4	-117.5
HKW5-61-1	102.0	117.2	23.9	20.4	3.5	137510.2	12810	80120.5	0.3	3.5	0.08	-155.9	507.1
HKW5-61-1	120.0	135.9	23.2	23.2	0.1	140857.9	223	91183.3		4.0	0.00	-556.9	-124.3
HKW5-61-1	99.0	113.9	22.4	22.4	0.1	135886.6	215	87965.1		3.8	0.00	-537.2	-119.9
HKW5-61-1	124.0	140.2	18.9	18.8	0.0	114243.8	180	73954.9		3.2	0.00	-451.7	-100.8
HKW5-61-1	119.0	134.9	19.6	19.5	0.1	118634.9	187	76797.4		3.3	0.00	-469.0	-104.7
HKW5-61-1	118.0	133.9	18.4	18.4	0.0	111758.0	177	72345.7		3.1	0.00	-441.8	-98.6
MKHD-W4	122.0	128.1	25.7	11.6	14.1	125959.1	51074	45601.3	1.3	2.0	0.39	1068.6	2427.5
MKHD-W4	120.0	126.0	25.3	13.4	11.9	128304.9	42908	52890.9	1.1	2.3	0.32	807.8	2017.8
MKHD-W4	123.0	129.1	25.2	13.7	11.5	128326.0	41596	53831.3	1.0	2.3	0.31	767.3	1952.3
MKHD-W4	122.0	128.0	25.1	14.4	10.7	129659.2	38653	56774.5	1.0	2.5	0.28	671.3	1804.2
MKHD-W4	120.0	126.0	23.5	9.1	14.4	111851.2	51922	35854.0	1.3	1.6	0.45	1151.2	2483.4
MKHD-W4	124.0	130.0	23.8	10.5	13.3	115836.2	47939	41251.5	1.2	1.8	0.40	1012.6	2280.8
MKHD-W4	122.0	128.0	23.3	9.4	13.9	111498.9	50140	36884.0	1.3	1.6	0.44	1097.7	2394.9
MKHD-W4	123.0	129.0	24.0	10.0	13.9	115707.7	50296	39503.5	1.3	1.7	0.42	1085.7	2398.6
MKHD-W-6-1	112.0	127.5	20.8	15.5	5.3	114907.5	19083	61032.7	0.5	2.7	0.15	127.8	841.8
MKHD-W-6-1	123.0	139.0	20.4	14.1	6.2	110303.0	22491	55639.6	0.6	2.4	0.19	251.1	1016.3
MKHD-W-6-1	114	129.6	21.4	16.0	5.4	118371.4	19658	62872.5	0.5	2.7	0.15	131.6	867.2
MKHD-W-6-1	111.0	126.5	20.8	14.3	6.6	112405.9	23750	56114.1	0.6	2.4	0.20	281.5	1077.1
MKHD-W-6-1	131.0	147.4	21.2	16.5	4.7	118642.3	16928	64977.2	0.4	2.8	0.13	46.4	730.7
MKHD-W-6-1	112.0	127.5	20.5	15.7	4.8	114084.2	17173	61847.8	0.4	2.7	0.14	72.2	747.3
MKHD-W4	117.0	132.7	21.5	16.0	5.5	118752.8	19722	63075.0	0.5	2.7	0.15	132.0	870.0
MKHD-W4	115	130.7	19.2	13.2	6.1	103666.2	21903	51751.1	0.5	2.3	0.20	259.6	993.3
MKHD-W4	113.0	128.6	19.7	14.5	5.2	108462.8	18846	57020.8	0.5	2.5	0.16	146.3	836.2
MKHD-W4	87.0	92.5	24.2	11.7	12.5	120070.5	45038	46046.3	1.1	2.0	0.36	906.3	2132.0
MKHD-W4	92.0	97.6	24.1	12.6	11.4	121657.5	41297	49718.0	1.0	2.2	0.32	784.8	1943.8
MKHD-W4	94.0	99.7	25.2	12.1	13.1	125025.8	47242	47702.9	1.2	2.1	0.36	954.4	2237.2
MKHD-W4	63.0	68.3	25.4	11.5	13.9	124680.5	50223	45373.6	1.3	2.0	0.39	1047.5	2386.3
MKHD-W4	87.0	92.6											
MKHD-W6-2	110.0	125.5	22.2	10.6	11.6	110151.8	41948	41797.4	1.0	1.8	0.37	850.9	1987.3
MKHD-W6-2	111.0	126.5	21.5	13.2	8.4	112685.1	30210	51731.8	0.8	2.3	0.25	479.3	1399.2
MKHD-W6-2	114.0	129.6	20.5	9.8	10.7	101654.4	38712	38573.1	1.0	1.7	0.37	785.2	1834.0
MKHD-W6-2	112.0	127.5	20.7	9.9	10.8	102591.9	39069	38928.8	1.0	1.7	0.37	792.5	1850.9
MKHD-W6-2	105.0	120.2	21.6	15.5	6.2	118111.3	22317	60825.7	0.6	2.6	0.17	214.5	1000.1
MKHD-W6-2	104.0	119.2	22.2	15.8	6.3	121052.2	22873	62340.2	0.6	2.7	0.17	219.9	1025.0
MKHD-W6-2	104.0	119.2	22.5	16.1	6.4	122872.6	23217	63277.7	0.6	2.8	0.17	223.2	1040.4
MKHD-W6-2	103.0	118.1	22.4	16.0	6.4	122145.9	23080	62903.5	0.6	2.7	0.17	221.8	1034.3
MKHD-W6-2	106.0	121.2	22.0	17.1	4.9	122936.1	17540	67328.8	0.4	2.9	0.13	48.1	757.1
MKHD-W6-2	103.0	118.1	21.6	18.7	3.0	124909.3	10767	73392.9	0.3	3.2	0.08	-168.4	417.2
MKHD-W6-2	108.0	123.4	22.3	13.6	8.7	116724.9	31293	53586.4	0.8	2.3	0.25	496.4	1449.3
MKHD-W6-2	103.0	118.1	21.5	12.8	8.7	111749.6	31474	50232.0	0.8	2.2	0.26	521.9	1463.2
MKHD-W6-2	110.0	125.4	21.4	12.0	9.4	109649.7	33771	47247.9	0.8	2.1	0.29	601.1	1579.8
MKHD-W6-2	101.0	116.0	21.3	14.4	6.9	114440.7	25018	56538.0	0.6	2.5	0.20	312.4	1138.4
MKHD-W6-2	107.0	122.3	20.1	10.7	9.4	102131.6	34040	42183.0	0.8	1.8	0.32	639.4	1600.4
MKHD-W6-2	104.0	119.1	20.5	11.2	9.3	104546.1	33535	44105.0	0.8	1.9	0.30	614.2	1572.9
MKHD-W6-2	106.0	121.2	21.2	12.8	8.4	110514.9	30381	50203.7	0.8	2.2	0.26	493.2	1409.8
MKHD-W-6-1	114.0	129.6	22.6	15.9	6.7	122621.2	24090	62498.1	0.6	2.7	0.18	251.0	1084.2
MKHD-W-6-1	127.0	143.2	22.1	12.1	10.0	112649.9	36135	47523.7	0.9	2.1	0.30	661.9	1694.9
MKHD-W-6-1	110.0	125.4	22.0	12.4	9.6	112893.5	34770	48645.7	0.9	2.1	0.29	618.9	1626.5
MKHD-W-6-1	103.0	118.1	22.1	15.3	6.7	119510.6	24368	60284.1	0.6	2.6	0.19	272.1	1101.1

Table S1.4c. Fluid inclusion data for dolomite-, dedolomite-, calcite- and quartz phases from Steltenberg quarry. Palaeooverburden thickness was compiled from Drozdzewski and Wrede (1994) and Götte (2004).

Sample	Mineral	Host	Estimated min. overburden [m]	FIA	Inclusion type	FI	Tm (I)	Th Halite	Th Halite corr.	Th hh corr.	Density
MKHD-W-6-1	dolomite	Dol 2B	4,000	cDol2B-1-5	cluster	5	-19.9	no halite	no halite	-25.1	1.12
HKW-5-63-1	dolomite	Dol 2B	4,000	cDol2B-1-1	cluster	1	-20.2	no halite	no halite	-23.3	1.11
HKW-5-63-1	dolomite	Dol 2B	4,000	cDol2B-1-2	cluster	2	-20.4	no halite	no halite	-23.6	1.11
HKW-5-63-1	dolomite	Dol 2B	4,000	cDol2B-1-3	cluster	3	-19.9	no halite	no halite	-25.4	1.10
HKW-5-63-1	dolomite	Dol 2B	4,000	cDol2B-1-4	cluster	4	-20.3	no halite	no halite	-23.8	1.11
HKW-5-63-1	dolomite	Dol 2B	4,000	cDol2B-1-5	cluster	5	-20.5	no halite	no halite	-22.9	1.11
HKW-5-63-1	dolomite	Dol 2B	4,000	cDol2B-1-6	cluster	6	-20.9	no halite	no halite	-25.3	1.12
HKW-63-5	dolomite	Dol 2B	4,000	cDol2B-1-1	cluster	1	-17.3	no halite	no halite	-23.3	1.11
HKW-63-5	dolomite	Dol 2B	4,000	cDol2B-1-2	cluster	2	-19.9	no halite	no halite	-23.2	1.12
HKW-63-5	dolomite	Dol 2B	4,000	cDol2B-1-3	cluster	3	-20.3	no halite	no halite	-23.4	1.12
HKW-63-5	dolomite	Dol 2B	4,000	cDol2B-1-4	cluster	4	-20.4	no halite	no halite	-23.3	1.12
HKW-63-5	dolomite	Dol 2B	4,000	cDol2B-1-5	cluster	5	-20.9	no halite	no halite	-24.9	1.12
HKW-63-5	dolomite	Dol 2B	4,000	cDol2B-1-6	cluster	6	-18.9	no halite	no halite	-25.4	1.12
HKW-63-5	dolomite	Dol 2B	4,000	cDol2B-1-7	cluster	7	-19.5	no halite	no halite	-26.2	1.12
HKW-63-5	dolomite	Dol 2B	4,000	cDol2B-1-8	cluster	8	-19.3	no halite	no halite	-22.7	1.12
HKW-63-5	dolomite	Dol 2B	4,000	cDol2B-1-9	cluster	9	-20.3	no halite	no halite	-23.9	1.12
MKHD-W6-2	calcite	LMC 1	3,000	pLMC1-1-2	primary	2	-14.9	no halite	no halite	no hh	0.99
MKHD-W6-2	calcite	LMC 1	3,000	pLMC1-1-3	primary	3	-14.8	no halite	no halite	no hh	0.99
MKHD-W6-2	calcite	LMC 1	3,000	pLMC1-1-4	primary	4	-10.6	no halite	no halite	no hh	0.98
MKHD-W6-2	calcite	LMC 1	3,000	pLMC1-1-5	primary	5	-12.6	no halite	no halite	no hh	0.99
MKHD-W6-2	calcite	LMC 1	3,000	pLMC1-2-1	primary	1	-13.3	no halite	no halite	no hh	no data
MKHD-W6-2	calcite	LMC 1	3,000	pLMC1-2-2	primary	2	-11.4	no halite	no halite	no hh	no data
MKHD-W6-2	calcite	LMC 1	3,000	pLMC1-2-3	primary	3	-13.2	no halite	no halite	no hh	no data
MKHD-W6-2	calcite	LMC 1	3,000	pLMC1-2-4	primary	4	-12.4	no halite	no halite	no hh	no data
MKHD-W6-2	calcite	LMC 1	3,000	pLMC1-2-5	primary	5	-13.7	no halite	no halite	no hh	no data
MKHD-W6-2	calcite	LMC 1	3,000	pLMC1-2-6	primary	6	-11.1	no halite	no halite	no hh	no data
MKHD-W4	dolomite	Dol 3A	1,000	pDol 3A-c-1	primary	1	-24.3	-35.40	metastable	no data	no data
MKHD-W4	dolomite	Dol 3A	1,000	pDol 3A-c-2	primary	2	-26.4	-32.80	metastable	no data	no data
MKHD-W4	dolomite	Dol 3A	1,000	pDol 3A-c-3	primary	3	-27.7	-31.00	metastable	no data	no data
MKHD-W4	dolomite	Dol 3A	1,000	pDol 3A-c-4	primary	4	-25	-34.90	metastable	no data	no data
HKW5-64-1	dolomite	Dol 3A	1,000	cDol3-1-1	cluster	1	-19.4	no halite	no halite	no hh	1.12
HKW5-64-1	dolomite	Dol 3A	1,000	cDol3-1-2	cluster	2	-20.3	no halite	no halite	no hh	1.11
HKW5-64-1	dolomite	Dol 3A	1,000	cDol3-1-3	cluster	3	-21	no halite	no halite	no hh	1.12
HKW5-64-1	dolomite	Dol 3A	1,000	cDol3-1-4	cluster	4	-20.7	no halite	no halite	no hh	1.11
HD-S-3-2	dolomite	Dol 3B	1,000	isoDol 3B-1-1	isolated	1	-19.7	no halite	no halite	no hh	1.07
HD-S-3-2	dolomite	Dol 3B	1,000	cDol 3B-1-1	cluster	1	-20.5	no halite	no halite	no hh	1.08
HD-S-3-2	dolomite	Dol 3B	1,000	cDol 3B-1-2	cluster	2	-20.9	no halite	no halite	no hh	1.09
HD-S-3-2	dolomite	Dol 3B	1,000	cDol 3B-1-3	cluster	3	-21	no halite	no halite	no hh	1.09
HD-S-3-2	dolomite	Dol 3B	1,000	cDol 3-1-1	cluster	1	-23.3	-32.40	metastable	no data	no data
HD-S-3-2	dolomite	Dol 3B	1,000	cDol 3-1-2	cluster	2	-26.8	-34.80	metastable	no data	no data
HD-S-3-2	dolomite	Dol 3B	1,000	cDol 3-1-3	cluster	3	-26.7	-33.00	metastable	no data	no data
HKW5-64-1	dolomite	Dol 3B	1,000	pDol 3B-1-1	primary	1	-19.5	no halite	no halite	no hh	1.08
HKW5-64-1	dolomite	Dol 3B	1,000	pDol 3B-1-2	primary	2	-18.2	no halite	no halite	no hh	1.08
HKW5-64-1	dolomite	Dol 3B	1,000	pDol 3B-1-3	primary	3	-17.4	no halite	no halite	no hh	1.07
HKW5-64-1	dolomite	Dol 3B	1,000	pDol 3B-1-4	primary	4	-18	no halite	no halite	no hh	1.08
HKW5-16-1	dolomite	Dol 3B	1,000	cDol 3B-1-1	cluster	1	-18.3	no halite	no halite	no hh	1.09
HKW5-16-1	dolomite	Dol 3B	1,000	cDol 3B-1-2	cluster	2	-17.9	no halite	no halite	no hh	1.09
HKW5-16-1	dolomite	Dol 3B	1,000	cDol 3B-1-3	cluster	3	-19.1	no halite	no halite	no hh	1.10
HKW5-16-1	dolomite	Dol 3B	1,000	cDol 3B-1-4	cluster	4	-18.4	no halite	no halite	no hh	1.10
HKW5-16-1	dolomite	Dol 3B	1,000	cDol 3B-1-5	cluster	5	-17.6	no halite	no halite	no hh	1.09
HKW5-16-1	dolomite	Dol 3B	1,000	cDol 3B-1-6	cluster	6	-18.3	no halite	no halite	no hh	1.10
HKW5-16-1	dolomite	Dol 3B	1,000	cDol 3B-1-7	cluster	7	-19.2	no halite	no halite	no hh	1.10
HKW 7-Lam1.1	dolomite	Lam 1 dol cc	1,000	pLam1-x-1	primary	1	-2	no halite	no halite	no hh	0.95
HKW 7-Lam1.1	dolomite	Lam 1 dol cc	1,000	pLam1-x-2	primary	2	-2.4	no halite	no halite	no hh	0.95
HKW 7-Lam1.1	dolomite	Lam 1 dol cc	1,000	pLam1-x-3	primary	3	-2.6	no halite	no halite	no hh	0.96

Table S1.4d. Fluid inclusion data for dolomite-, dedolomite-, calcite- and quartz phases from Steltenberg quarry. Palaeooverburden thickness was compiled from Drozdzewski and Wrede (1994) and Götte (2004).

Sample	T_h uncorr.	T_h corr.	Salinity	NaCl wt.%	CaCl$_2$ wt.%	Cl ppm	Ca ppm	Na ppm	Mole Ca	Mole Na	Mole ratio Ca/(Na+Ca)	Na deficit	Ca excess
MKHD-W-6-1	109.0	124.4	21.5	12.3	9.2	110736.9	33388	48223.9	0.8	2.1	0.28	584.9	1559.6
HKW-5-63-1	115.0	130.7	22.0	16.2	5.8	121160.8	21053	63696.3	0.5	2.8	0.16	163.4	934.1
HKW-5-63-1	114.0	129.6	22.1	15.6	6.5	120093.3	23593	61209.7	0.6	2.7	0.18	245.9	1061.9
HKW-5-63-1	127.0	143.2	21.5	11.7	9.7	109459.9	35112	46177.9	0.9	2.0	0.30	643.1	1646.9
HKW-5-63-1	114.0	129.6	22.0	15.0	6.9	118580.9	25054	59196.7	0.6	2.6	0.20	296.9	1136.3
HKW-5-63-1	117.0	132.8	22.3	17.4	4.9	124864.3	17815	68384.8	0.4	3.0	0.13	48.9	769.0
HKW-5-63-1	110.0	125.5	22.1	12.3	9.8	113088.5	35557	48216.6	0.9	2.1	0.30	642.3	1665.6
HKW-63-5	100.0	115.0	20.0	14.7	5.3	110052.0	19123	57856.3	0.5	2.5	0.16	148.4	848.4
HKW-63-5	104.0	119.2	21.8	16.3	5.5	120649.8	20037	64082.6	0.5	2.8	0.15	134.1	883.9
HKW-63-5	107.0	122.3	22.1	16.0	6.1	120921.5	21933	62919.2	0.5	2.7	0.17	191.4	978.3
HKW-63-5	104.0	119.2	22.2	16.3	5.9	121905.7	21182	64088.0	0.5	2.8	0.16	164.4	939.8
HKW-63-5	107.0	122.3	22.2	13.0	9.2	114924.3	33137	51116.5	0.8	2.2	0.27	560.4	1543.1
HKW-63-5	99.0	113.9	20.8	11.4	9.4	106203.3	34067	44804.1	0.9	1.9	0.30	624.0	1597.9
HKW-63-5	97.0	112.0	21.1	10.4	10.8	105137.5	38829	40749.0	1.0	1.8	0.35	774.9	1836.5
HKW-63-5	102.0	117.0	21.5	17.3	4.3	121495.9	15406	67902.6	0.4	3.0	0.12	-11.8	652.0
HKW-63-5	103.0	118.0	22.0	14.8	7.1	118021.7	25800	58307.1	0.6	2.5	0.20	322.1	1174.0
MKHD-W6-2	224.0	228.5	18.4	18.4	0.0	111758.0	177	72345.7		3.1	0.00	-441.8	-98.6
MKHD-W6-2	221.0	225.5	18.4	18.3	0.0	111256.4	176	72021.0		3.1	0.00	-439.8	-98.2
MKHD-W6-2	195.0	199.7	14.6	14.6	0.0	88424.6	140	57241.0		2.5	0.00	-349.6	-78.0
MKHD-W6-2	207.0	211.7	16.5	16.4	0.0	99784.2	158	64594.5		2.8	0.00	-394.5	-88.0
MKHD-W6-2	202.0	206.1	17.1	17.0	0.0	103534.2	164	67022.1		2.9	0.00	-409.3	-91.3
MKHD-W6-2	214.0	218.3	15.4	15.3	0.0	93094.8	147	60264.2		2.6	0.00	-368.0	-82.1
MKHD-W6-2	218.0	222.4	17.0	17.0	0.0	103004.7	163	66679.3		2.9	0.00	-407.2	-90.9
MKHD-W6-2	208.0	212.2	16.3	16.2	0.0	98693.3	156	63888.3		2.8	0.00	-390.2	-87.1
MKHD-W6-2	200.0	204.0	17.4	17.4	0.0	105632.6	167	68380.5		3.0	0.00	-417.6	-93.2
MKHD-W6-2	204.0	208.1	15.1	15.0	0.0	91364.7	144	59144.2		2.6	0.00	-361.2	-80.6
MKHD-W4	82.0	no data	no data	no data	no data	no data	no data	no data	no data	no data	no data	no data	no data
MKHD-W4	82.0	no data	no data	no data	no data	no data	no data	no data	no data	no data	no data	no data	no data
MKHD-W4	81.0	no data	no data	no data	no data	no data	no data	no data	no data	no data	no data	no data	no data
MKHD-W4	83.0	no data	no data	no data	no data	no data	no data	no data	no data	no data	no data	no data	no data
HKW5-64-1	99.0	102.7	22.0	21.9	0.1	133152.6	210	86195.3		3.7	0.00	-526.4	-117.5
HKW5-64-1	113.0	116.9	22.6	22.6	0.1	137247.2	217	88845.9		3.9	0.00	-542.6	-121.1
HKW5-64-1	111.0	114.8	23.2	23.1	0.1	140407.8	222	90891.9		4.0	0.00	-555.1	-123.9
HKW5-64-1	117.0	120.9	22.9	22.9	0.1	139055.5	220	90016.5		3.9	0.00	-549.7	-122.7
HD-S-3-2	161.0	165.3	22.2	22.1	0.1	134521.8	212	87081.7		3.8	0.00	-531.8	-118.7
HD-S-3-2	155.0	159.2	22.8	22.7	0.1	138152.1	218	89431.7		3.9	0.00	-546.2	-121.9
HD-S-3-2	152.0	156.2	23.1	23.0	0.1	139957.4	221	90600.4		3.9	0.00	-553.3	-123.5
HD-S-3-2	156.0	160.3	23.2	23.1	0.1	140407.8	222	90891.9		4.0	0.00	-555.1	-123.9
HD-S-3-2	87.0	no data	no data	no data	no data	no data	no data	no data	no data	no data	no data	no data	no data
HD-S-3-2	82.0	no data	no data	no data	no data	no data	no data	no data	no data	no data	no data	no data	no data
HD-S-3-2	89.0	no data	no data	no data	no data	no data	no data	no data	no data	no data	no data	no data	no data
HKW5-64-1	149.0	153.2	22.0	22.0	0.1	133609.5	211	86491.1		3.8	0.00	-528.2	-117.9
HKW5-64-1	148.0	152.2	21.1	21.0	0.1	127622.6	202	82615.5		3.6	0.00	-504.5	-112.6
HKW5-64-1	149.0	153.2	20.4	20.4	0.1	123878.6	196	80191.9		3.5	0.00	-489.7	-109.3
HKW5-64-1	147.0	151.2	20.9	20.8	0.1	126691.4	200	82012.7		3.6	0.00	-500.9	-111.8
HKW5-16-1	132.0	136.0	21.1	21.1	0.1	128087.1	202	82916.2		3.6	0.00	-506.4	-113.0
HKW5-16-1	122.0	125.9	20.8	20.8	0.1	126224.7	199	81710.6		3.6	0.00	-499.0	-111.4
HKW5-16-1	128.0	132.0	21.7	21.7	0.1	131778.5	208	85305.8		3.7	0.00	-521.0	-116.3
HKW5-16-1	124.0	128.0	21.2	21.2	0.1	128550.9	203	83216.4		3.6	0.00	-508.2	-113.4
HKW5-16-1	130.0	134.0	20.6	20.5	0.1	124819.6	197	80801.0		3.5	0.00	-493.5	-110.1
HKW5-16-1	119.0	122.9	21.1	21.1	0.1	128087.1	202	82916.2		3.6	0.00	-506.4	-113.0
HKW5-16-1	125.0	129.0	21.8	21.8	0.1	132237.1	209	85602.7		3.7	0.00	-522.8	-116.7
HKW 7-Lam1.1	220.0	225.3	3.4	3.4	0.0	20539.5	32	13296.1	0.0	0.6	0.00	-81.2	-18.1
HKW 7-Lam1.1	220.0	225.3	4.0	4.1	0.0	24710.8	39	15996.3	0.0	0.7	0.00	-97.7	-21.8
HKW 7-Lam1.1	214.0	219.3	4.3	4.4	0.0	26748.1	42	17315.2	0.0	0.8	0.00	-105.7	-23.6

Table S1.4e. Fluid inclusion data for dolomite-, dedolomite-, calcite- and quartz phases from Steltenberg quarry. Palaeooverburden thickness was compiled from Drozdzewski and Wrede (1994) and Götte (2004).

Sample	Mineral	Host	Estimated min. overburden [m]	FIA	Inclusion type	FI	Tm (I)	Th Halite	Th Halite corr.	Th hh corr.	Density
HKW 7-Lam1.1	dolomite	Lam 1 dol cc	1,000	pLam1-x-4	primary	4	-1.7	no halite	no halite	no hh	0.97
HKW 7-Lam1.1	dolomite	Lam 1 dol cc	1,000	pLam1-x-5	primary	5	-2	no halite	no halite	no hh	0.96
HKW 7-Lam1.1	dolomite	Lam 1 dol cc	1,000	pLam1-x-1	primary	1	-4	no halite	no halite	no hh	0.97
HKW 7-Lam1.1	dolomite	Lam 1 dol cc	1,000	pLam1-x-2	primary	2	-1.9	no halite	no halite	no hh	0.95
HKW 7-Lam1.1	dolomite	Lam 1 dol cc	1,000	pLam1-x-3	primary	3	-3.6	no halite	no halite	no hh	0.97
HKW 7-Lam1.1	dolomite	Lam 1 dol cc	1,000	pLam1-x-4	primary	4	-3	no halite	no halite	no hh	0.95
HKW 7-Lam1.1	dolomite	Lam 1 dol cc	1,000	sLam1-1	secondary	1	no data	no halite	no halite	no hh	no data
HKW 7-Lam1.1	dolomite	Lam 1 dol cc	1,000	sLam1-2	secondary	2	no data	no halite	no halite	no hh	no data
HKW 7-Lam1.1	dolomite	Lam 1 dol cc	1,000	sLam1-3	secondary	3	no data	no halite	no halite	no hh	no data
HKW 7-Lam1.1	dolomite	Lam 1 dol cc	1,000	sLam1-4	secondary	4	no data	no halite	no halite	no hh	no data
HKW5-16-1	calcite	Dedol 2	1,000	Dedol2-1-1	cluster	1	-5.2	no halite	no halite	no hh	1.00
HKW5-16-1	calcite	Dedol 2	1,000	Dedol2-1-2	cluster	2	-4.1	no halite	no halite	no hh	0.99
HD-S-3-2	calcite	Dedol 2	1,000	cDedol 2-1-1	cluster	1	-8.3	no halite	no halite	no hh	1.02
HD-S-3-2	calcite	Dedol 2	1,000	cDedol 2-1-2	cluster	2	-9.4	no halite	no halite	no hh	1.04
HD-S-3-2	calcite	Dedol 2	1,000	cDedol 2-1-3	cluster	3	-10.3	no halite	no halite	no hh	1.04
HD-S-3-2	calcite	Dedol 2	1,000	cDedol 2-1-4	cluster	4	-8.9	no halite	no halite	no hh	1.02
HD-S-3-2	quartz	Qz 2A	1,000	pQz 2A-1-1	primary	1	-20.1	no halite	no halite	-23.2	1.11
HD-S-3-2	quartz	Qz 2A	1,000	pQz 2A-1-2	primary	2	-20.4	no halite	no halite	-23.7	1.12
HD-S-3-2	quartz	Qz 2A	1,000	pQz 2A-1-3	primary	3	-20.6	no halite	no halite	-23	1.12
HD-S-3-2	quartz	Qz 2A	1,000	pQz 2A-1-4	primary	4	-20.6	no halite	no halite	-23.8	1.12
HD-S-3-2	quartz	Qz 2A	1,000	pQz 2A-3-1	primary	1	-20.3	no halite	no halite	-22.8	1.11
HD-S-3-2	quartz	Qz 2A	1,000	pQz 2A-3-2	primary	2	-20.5	no halite	no halite	-23.7	1.12
HD-S-3-2	quartz	Qz 2A	1,000	pQz 2A-3-3	primary	3	-20.3	no halite	no halite	-23.3	1.12
HD-S-3-2	quartz	Qz 2A	1,000	pQz 2A-3-4	primary	4	-21.1	no halite	no halite	-22.8	1.12
HKW5-64-1	quartz	Qz 2A	1,000	pQz2A-1-1	cluster	1	-20.4	no halite	no halite	-23.3	1.11
HKW5-64-1	quartz	Qz 2A	1,000	pQz2A-1-2	cluster	2	-20.6	no halite	no halite	-23.2	1.11
HKW5-64-1	quartz	Qz 2A	1,000	pQz2A-1-3	cluster	3	-19.9	no halite	no halite	-23.8	1.11
HD-S-3-2	quartz	Qz 2B	1,000	pQz 2B-1-1	primary	1	-24.7	no halite	no halite	-26.5	1.15
HD-S-3-2	quartz	Qz 2B	1,000	pQz 2B-1-2	primary	2	-24.5	no halite	no halite	-26.6	1.15
HD-S-3-2	quartz	Qz 2B	1,000	pQz 2B-1-3	primary	3	-19.6	no halite	no halite	-25.5	1.13
HD-S-3-2	quartz	Qz 2B	1,000	pQz 2B-1-4	primary	4	-20.1	no halite	no halite	-26.8	1.13
HD-S-3-2	quartz	Qz 2B	1,000	pQz 2B-1-5	primary	5	-20.5	no halite	no halite	-25.2	1.13
HD-S-3-2	quartz	Qz 2B	1,000	pQz 2B-1-6	primary	6	-20.4	no halite	no halite	-25.8	1.13
HD-S-3-2	quartz	Qz 2B	1,000	pQz 2B-1-7	primary	7	-19.6	no halite	no halite	-27.7	1.13
HD-S-3-2	quartz	Qz 2B	1,000	pQz 2B-1-8	primary	8	-19.6	no halite	no halite	-24.9	1.12
HD-S-3-2	quartz	Qz 2B	1,000	pQz 2B-1-9	primary	9	-21.1	no halite	no halite	-27.3	1.13
HD-S-3-2	quartz	Qz 2B	1,000	pQz 2B-1-10	primary	10	-20.2	no halite	no halite	-26.4	1.13
HD-S-3-2	quartz	Qz 2B	1,000	pQz 2A-2-1	primary	1	-19.4	no halite	no halite	-23.1	1.11
HD-S-3-2	quartz	Qz 2B	1,000	pQz 2A-2-2	primary	2	-20.3	no halite	no halite	-23.3	1.11
HD-S-3-2	quartz	Qz 2B	1,000	pQz 2A-2-3	primary	3	-20.4	no halite	no halite	-23.2	1.11
HD-S-3-2	quartz	Qz 2B	1,000	pQz 2A-2-4	primary	4	-20.7	no halite	no halite	-23.8	1.12
HKW5-64-1	quartz	Qz 2B	1,000	cQz2B-1-1	cluster	1	-25	no halite	no halite	-24.8	1.15
HKW5-64-1	quartz	Qz 2B	1,000	cQz2B-1-2	cluster	2	-25.1	no halite	no halite	-25.2	1.15
HKW5-64-1	quartz	Qz 2B	1,000	cQz2B-1-3	cluster	3	-25.4	no halite	no halite	-26.3	1.15
HKW5-64-1	quartz	Qz 2B	1,000	cQz2B-1-4	cluster	4	-24.9	no halite	no halite	-25	1.15
HKW 8-LMC 3	calcite	LMC 3	1,000	pLMC3-x-1	primary	1	-20.9	no halite	no halite	no hh	decrap
HKW 8-LMC 3	calcite	LMC 3	1,000	pLMC3-x-2	primary	2	-2.5	no halite	no halite	no hh	decrap
HKW 8-LMC 3	calcite	LMC 3	1,000	pLMC3-x-3	primary	3	-22	no halite	no halite	no hh	1.15
HKW 8-LMC 3	calcite	LMC 3	1,000	pLMC3-x-4	primary	4	-3.2	no halite	no halite	no hh	1.01
HKW 8-LMC 3	calcite	LMC 3	1,000	pLMC3-x-5	primary	5	-21.2	no halite	no halite	no hh	1.14
HKW 8-LMC 3	calcite	LMC 3	1,000	pLMC3-x-6	primary	6	-3.8	no halite	no halite	no hh	1.01
HKW 8-LMC 3	calcite	LMC 3	1,000	pLMC3-x-1	primary	1	0	no halite	no halite	no hh	0.97
HKW 8-LMC 3	calcite	LMC 3	1,000	pLMC3-x-2	primary	2	-4	no halite	no halite	no hh	1.01
HKW 8-LMC 3	calcite	LMC 3	1,000	pLMC3-x-3	primary	3	-23	no halite	no halite	no hh	1.15
HKW 8-LMC 3	calcite	LMC 3	1,000	pLMC3-x-4	primary	4	-20	no halite	no halite	no hh	1.13

Table S1.4f. Fluid inclusion data for dolomite-, dedolomite-, calcite- and quartz phases from Steltenberg quarry. Palaeooverburden thickness was compiled from Drozdzewski and Wrede (1994) and Götte (2004).

Sample	Th uncorr.	Th corr.	Salinity	NaCl wt.%	CaCl2 wt.%	Cl ppm	Ca ppm	Na ppm	Mole Ca	Mole Na	Mole ratio Ca/(Na+Ca)	Na deficit	Ca excess
HKW 7-Lam1.1	215.0	220.3	2.9	2.9	0.0	17323.9	27	11214.5	0.0	0.5	0.00	-68.5	-15.3
HKW 7-Lam1.1	221.0	226.3	3.4	3.4	0.0	20539.5	32	13296.1	0.0	0.6	0.00	-81.2	-18.1
HKW 7-Lam1.1	209.0	214.3	6.4	6.6	0.0	40165.2	63	26000.6	0.0	1.1	0.00	-158.8	-35.4
HKW 7-Lam1.1	207.0	212.4	3.2	3.2	0.0	19476.0	31	12607.7	0.0	0.5	0.00	-77.0	-17.2
HKW 7-Lam1.1	209.0	214.3	5.9	6.0	0.0	36476.3	58	23612.7	0.0	1.0	0.00	-144.2	-32.2
HKW 7-Lam1.1	208.0	213.3	5.0	5.1	0.0	30729.2	49	19892.3	0.0	0.9	0.00	-121.5	-27.1
HKW 7-Lam1.1	165.0	no data	no data	no data	no data	no data	no data	no data	no data	no data	no data	no data	no data
HKW 7-Lam1.1	180.0	no data	no data	no data	no data	no data	no data	no data	no data	no data	no data	no data	no data
HKW 7-Lam1.1	180.0	no data	no data	no data	no data	no data	no data	no data	no data	no data	no data	no data	no data
HKW 7-Lam1.1	175.0	no data	no data	no data	no data	no data	no data	no data	no data	no data	no data	no data	no data
HKW5-16-1	125.0	129.7	8.3	8.3	0.0	50598.1	80	32754.3		1.4	0.00	-200.0	-44.6
HKW5-16-1	126.0	130.8	6.8	6.8	0.0	41070.2	65	26586.5		1.2	0.00	-162.4	-36.2
HD-S-3-2	125.0	129.3	12.2	12.2	0.0	73840.8	117	47800.3		2.1	0.00	-291.9	-65.2
HD-S-3-2	123.0	127.2	13.4	13.3	0.0	81050.1	128	52467.2		2.3	0.00	-320.4	-71.5
HD-S-3-2	122.0	126.1	14.3	14.3	0.0	86624.7	137	56075.8		2.4	0.00	-342.5	-76.4
HD-S-3-2	132.0	136.4	12.8	12.8	0.0	77830.6	123	50383.0		2.2	0.00	-307.7	-68.7
HD-S-3-2	112.0	115.8	22.0	16.4	5.6	121404.4	20162	64483.4	0.5	2.8	0.15	135.0	889.4
HD-S-3-2	113.0	116.9	22.1	15.3	6.7	119510.6	24368	60284.1	0.6	2.6	0.19	272.1	1101.1
HD-S-3-2	112.0	115.8	22.4	17.2	5.2	124580.8	18754	67538.2	0.5	2.9	0.14	78.9	816.1
HD-S-3-2	111.0	114.8	22.2	15.2	7.0	119651.8	25281	59731.3	0.6	2.6	0.20	299.6	1146.5
HD-S-3-2	114.0	117.9	22.2	17.5	4.7	124764.0	16814	69027.1	0.4	3.0	0.12	18.4	719.1
HD-S-3-2	109.0	112.8	22.1	15.4	6.8	119870.4	24442	60465.6	0.6	2.6	0.19	272.9	1104.4
HD-S-3-2	112.0	115.8	22.1	16.2	5.8	121533.5	21118	63892.3	0.5	2.8	0.16	163.9	937.0
HD-S-3-2	112.0	115.9	22.8	18.0	4.8	127858.1	17231	70738.9	0.4	3.1	0.12	18.9	736.9
HKW5-64-1	121.0	124.9	22.2	16.3	5.9	121905.7	21182	64088.0	0.5	2.8	0.16	164.4	939.8
HKW5-64-1	118.0	121.9	22.3	16.6	5.7	123281.1	20474	65480.3	0.5	2.8	0.15	137.1	903.2
HKW5-64-1	121.0	124.9	21.7	14.9	6.9	117145.0	24751	58479.9	0.6	2.5	0.20	293.3	1122.5
HD-S-3-2	89.0	92.7	24.1	11.4	12.8	119212.6	46073	44759.1	1.1	1.9	0.37	941.6	2184.5
HD-S-3-2	92.0	95.7	24.0	11.2	12.8	118238.6	46358	43926.0	1.2	1.9	0.38	954.3	2199.7
HD-S-3-2	87.0	90.6	21.3	11.5	9.8	108085.9	35351	45117.8	0.9	2.0	0.31	656.0	1660.1
HD-S-3-2	94.0	97.7	21.4	9.7	11.7	104919.8	42292	38162.0	1.1	1.7	0.39	882.4	2009.5
HD-S-3-2	90.0	93.6	21.9	12.3	9.6	112249.6	34572	48368.2	0.9	2.1	0.29	615.3	1617.3
HD-S-3-2	96.0	99.7	21.7	11.2	10.5	109424.3	37812	44247.2	0.9	1.9	0.33	726.4	1781.7
HD-S-3-2	90.0	93.6	21.0	8.5	12.5	100774.6	45318	33336.4	1.1	1.5	0.44	992.1	2164.5
HD-S-3-2	101.0	104.7	21.3	12.5	8.8	110626.2	31897	49204.8	0.8	2.1	0.27	539.5	1485.4
HD-S-3-2	99.0	102.7	21.9	9.3	12.6	106211.0	45624	36645.3	1.1	1.6	0.42	979.8	2174.6
HD-S-3-2	91.0	94.6	21.5	10.3	11.2	106574.1	40586	40439.9	1.0	1.8	0.37	823.2	1922.8
HD-S-3-2	113.0	116.9	21.5	16.3	5.2	119358.7	18898	64049.7	0.5	2.8	0.14	104.2	828.3
HD-S-3-2	118.0	121.9	22.1	16.2	5.8	121533.5	21118	63892.3	0.5	2.8	0.16	163.9	937.0
HD-S-3-2	124.0	128.0	22.2	16.5	5.6	122532.0	20349	65082.4	0.5	2.8	0.15	136.2	897.7
HD-S-3-2	103.0	106.8	22.3	15.2	7.0	120007.7	25356	59908.9	0.6	2.6	0.20	300.5	1149.9
HKW5-64-1	93.0	96.7	24.7	14.3	10.4	127568.9	37552	56196.9	0.9	2.4	0.28	645.8	1751.2
HKW5-64-1	97.0	100.8	24.7	13.9	10.8	126605.7	38993	54554.2	1.0	2.4	0.29	694.0	1824.1
HKW5-64-1	92.0	95.7	24.6	11.9	12.7	122044.6	45779	46803.4	1.1	2.0	0.36	921.2	2167.1
HKW5-64-1	98.0	101.8	24.6	14.2	10.4	127093.1	37486	55934.9	0.9	2.4	0.28	645.7	1748.4
HKW 8-LMC 3	decrap	decrap	decrap	23.0	0.1	139957.4	221	90600.4	0.0	3.9	0.00	-553.3	-123.5
HKW 8-LMC 3	decrap	decrap	decrap	4.2	0.0	25733.4	41	16658.3	0.0	0.7	0.00	-101.7	-22.7
HKW 8-LMC 3	76.0	79.5	23.7	21.1	2.6	138491.4	9545	83063.3	0.2	3.6	0.06	-260.3	343.2
HKW 8-LMC 3	83.0	87.6	5.3	5.4	0.0	32674.2	52	21151.4	0.0	0.9	0.00	-129.2	-28.8
HKW 8-LMC 3	80.0	83.5	23.2	23.3	0.1	141307.7	223	91474.4	0.0	4.0	0.00	-558.7	-124.7
HKW 8-LMC 3	84.0	88.5	6.2	6.3	0.0	38334.6	61	24815.6	0.0	1.1	0.00	-151.6	-33.8
HKW 8-LMC 3	84.5	89.8	0.0	-0.4	0.0	-2424.1	-4	-1569.3	0.0	-0.1	0.00	9.6	2.1
HKW 8-LMC 3	82.0	86.4	6.4	6.6	0.0	40165.2	63	26000.6	0.0	1.1	0.00	-158.8	-35.4
HKW 8-LMC 3	85.0	88.6	24.3	18.7	5.5	135382.3	19961	73689.7	0.5	3.2	0.13	72.8	865.9
HKW 8-LMC 3	87.5	91.1	22.4	22.4	0.1	135886.6	215	87965.1	0.0	3.8	0.00	-537.2	-119.9

Table S1.4g. Fluid inclusion data for dolomite-, dedolomite-, calcite- and quartz phases from Steltenberg quarry. Palaeooverburden thickness was compiled from Drozdzewski and Wrede (1994) and Götte (2004).

Sample	Mineral	Host	Estimated min. overburden [m]	FIA	Inclusion type	FI	Tm (I)	Th Halite	Th Halite corr.	Th hh corr.	Density
HKW 8-LMC 3	calcite	LMC 3	1,000	pLMC3-x-5	primary	5	-20.5	no halite	no halite	no hh	1.13
HKW 8-LMC 3	calcite	LMC 3	unknown	sLMC3-1	Secondary	1	-6.1	no halite	no halite	-19.5	0.92
HKW 8-LMC 3	calcite	LMC 3	1,000	pLMC3-x-1	primary	1	-3.7	no halite	no halite	no hh	1.01
HKW 8-LMC 3	calcite	LMC 3	1,000	pLMC3-x-2	primary	2	-21	no halite	no halite	no hh	1.13
HKW 8-LMC 3	calcite	LMC 3	1,000	pLMC3-x-3	primary	3	-20.8	no halite	no halite	no hh	1.13
HKW 8-LMC 3	calcite	LMC 3	1,000	pLMC3-x-4	primary	4	-19.9	no halite	no halite	no hh	1.13
HKW 8-LMC 3	calcite	LMC 3	1,000	pLMC3-x-5	primary	5	-20.8	no halite	no halite	no hh	1.14
HKW 8-LMC 3	calcite	LMC 3	1,000	pLMC3-x-6	primary	6	-4	no halite	no halite	no hh	1.01
HKW 8-LMC 3	calcite	LMC 3	1,000	pLMC3-x-7	primary	7	-3.2	no halite	no halite	no hh	1.01
HKW 8-LMC 3	calcite	LMC 3	1,000	pLMC3-x-1	primary	1	-2.8	no halite	no halite	no hh	1.00
HKW 8-LMC 3	calcite	LMC 3	1,000	pLMC3-x-2	primary	2	-2.9	no halite	no halite	no hh	1.00
HKW 8-LMC 3	calcite	LMC 3	1,000	pLMC3-x-3	primary	3	-21.1	no halite	no halite	no hh	1.13
HKW 8-LMC 3	calcite	LMC 3	1,000	pLMC3-x-4	primary	4	-3.3	no halite	no halite	no hh	1.00
HKW 8-LMC 3	calcite	LMC 3	1,000	pLMC3-x-5	primary	5	-2.7	no halite	no halite	no hh	0.99
HKW 8-LMC 3	calcite	LMC 3	1,000	pLMC3-x-6	primary	6	-21.2	no halite	no halite	no hh	1.14
MKHD-W6-2	calcite	LMC 4	1,500	pLMC 4-2-1	primary	1	-3.2	no halite	no halite	no hh	0.98
MKHD-W6-2	calcite	LMC 4	1,500	pLMC 4-2-2	primary	2	-3.1	no halite	no halite	no hh	0.97
MKHD-W6-2	calcite	LMC 4	1,500	pLMC 4-2-3	primary	3	-3.4	no halite	no halite	no hh	0.98
MKHD-W6-2	calcite	LMC 4	1,500	pLMC 4-2-4	primary	4	-3.5	no halite	no halite	no hh	0.98
MKHD-W-6-1	calcite	LMC 5	1,000	pLMC5-1-1	primary	1	-28.3	no halite	no halite	-25.3	1.17
MKHD-W-6-1	calcite	LMC 5	1,000	pLMC5-1-2	primary	2	-29	no halite	no halite	-26.7	1.17
MKHD-W-6-1	calcite	LMC 5	1,000	pLMC5-1-3	primary	3	-28.7	no halite	no halite	-26.8	1.17
MKHD-W-6-1	calcite	LMC 5	1,000	pLMC5-1-4	primary	4	-24	no halite	no halite	-23.9	1.15
MKHD-W-6-1	calcite	LMC 5	1,000	pLMC5-1-5	primary	5	-26.7	no halite	no halite	-24.8	1.16
MKHD-W-6-1	calcite	LMC 5	1,000	pLMC5-1-6	primary	6	-27.6	no halite	no halite	-24.5	1.16
MKHD-W-6-1	calcite	LMC 5	1,000	pLMC5-1-7	primary	7	-25.6	no halite	no halite	-25.6	1.16
HKW 7-CZ2.1	calcite	LMC 6A	1,000	pLMC6A-x-1	primary	1	-15.7	no halite	no halite	no hh	1.12
HKW 7-CZ2.1	calcite	LMC 6A	1,000	pLMC6A-x-2	primary	2	-14.8	no halite	no halite	no hh	1.12
HKW 7-CZ2.1	calcite	LMC 6A	1,000	pLMC6A-x-3	primary	3	-16.8	no halite	no halite	no hh	1.13
HKW 7-CZ2.1	calcite	LMC 6A	1,000	pLMC6A-x-4	primary	4	-16.6	no halite	no halite	no hh	1.13
HKW 7-CZ2.1	calcite	LMC 6A	1,000	pLMC6A-x-5	primary	5	-15.5	no halite	no halite	no hh	1.12
HKW 7-CZ2.1	calcite	LMC 6B	1,000	pLMC6B-x-1	primary	1	-14	no halite	no halite	no hh	1.11
HKW 7-CZ2.1	calcite	LMC 6B	1,000	pLMC6B-x-2	primary	2	-14.8	no halite	no halite	no hh	1.12
HKW 7-CZ2.1	calcite	LMC 6B	1,000	pLMC6B-x-3	primary	3	-13.3	no halite	no halite	no hh	1.11
HKW 7-CZ2.1	calcite	LMC 6B	1,000	pLMC6B-x-4	primary	4	-13.5	no halite	no halite	no hh	1.11
HKW 7-CZ2.1	calcite	LMC 6B	1,000	pLMC6B-x-5	primary	5	-13.3	no halite	no halite	no hh	1.11
HKW 7-CZ2.1	calcite	LMC 6B	1,000	pLMC6B-x-1	primary	1	-15.5	no halite	no halite	no hh	1.12
HKW5-64-1	calcite	LMC 6	1,000	cLMC6-1-1	cluster	1	-11.1	no halite	no halite	no hh	1.00
HKW5-64-1	calcite	LMC 6	1,000	cLMC6-1-2	cluster	2	-12.3	no halite	no halite	no hh	1.00
HKW5-64-1	calcite	LMC 6	1,000	cLMC6-1-3	cluster	3	-11.9	no halite	no halite	no hh	1.01
HKW5-64-1	calcite	LMC 6	1,000	cLMC6-1-4	cluster	5	-14.3	no halite	no halite	no hh	1.05
HKW5-16-1	calcite	LMC 7	1,000	cLMC2-1-1	cluster	1	-13.1	no halite	no halite	no hh	1.06
HKW5-16-1	calcite	LMC 7	1,000	cLMC2-1-2	cluster	2	-14.2	no halite	no halite	no hh	1.07
HKW5-16-1	calcite	LMC 7	1,000	cLMC2-1-3	cluster	3	-14.5	no halite	no halite	no hh	1.07
HKW5-16-1	calcite	LMC 7	1,000	cLMC2-1-4	cluster	4	-12.9	no halite	no halite	no hh	1.06
HKW 7-Lam1.1	calcite	LMC 8	1,000	pLMC8-x-1	primary	1	-12.7	no halite	no halite	no hh	1.03
HKW 7-Lam1.1	calcite	LMC 8	1,000	pLMC8-x-2	primary	2	-12.3	no halite	no halite	no hh	1.02
HKW 7-Lam1.1	calcite	LMC 8	1,000	pLMC8-x-3	primary	3	-13.2	no halite	no halite	no hh	1.01
HKW 7-Lam1.1	calcite	LMC 8	1,000	pLMC8-x-4	primary	4	-11.2	no halite	no halite	no hh	0.99
HKW 7-Lam1.1	calcite	LMC 8	1,000	pLMC8-x-5	primary	5	-11.8	no halite	no halite	no hh	1.00

Table S1.4h. Fluid inclusion data for dolomite-, dedolomite-, calcite- and quartz phases from Steltenberg quarry. Palaeooverburden thickness was compiled from Drozdzewski and Wrede (1994) and Götte (2004).

Sample	T_h uncorr.	T_h corr.	Salinity	NaCl wt.%	CaCl$_2$ wt.%	Cl ppm	Ca ppm	Na ppm	Mole Ca	Mole Na	Mole ratio Ca/(Na+Ca)	Na deficit	Ca excess
HKW 8-LMC 3	84.0	87.6	22.7	22.7	0.1	138152.1	218	89431.7	0.0	3.9	0.00	-546.2	-121.9
HKW 8-LMC 3	219.0	224.0	9.3	9.5	0.0	57853.1	91	37450.8	0.0	1.6	0.00	-228.7	-51.0
HKW 8-LMC 3	92.3	96.9	6.0	6.2	0.0	37409.0	59	24216.4	0.0	1.1	0.00	-147.9	-33.0
HKW 8-LMC 3	90.2	93.8	23.0	23.1	0.1	140407.8	222	90891.9	0.0	4.0	0.00	-555.1	-123.9
HKW 8-LMC 3	88.3	91.9	22.9	23.0	0.1	139506.6	220	90308.6	0.0	3.9	0.00	-551.5	-123.1
HKW 8-LMC 3	87.5	91.1	22.3	22.3	0.1	135432.1	214	87670.9	0.0	3.8	0.00	-535.4	-119.5
HKW 8-LMC 3	80.3	83.8	22.9	23.0	0.1	139506.6	220	90308.6	0.0	3.9	0.00	-551.5	-123.1
HKW 8-LMC 3	86.3	90.8	6.4	6.6	0.0	40165.2	63	26000.6	0.0	1.1	0.00	-158.8	-35.4
HKW 8-LMC 3	80.8	85.4	5.3	5.4	0.0	32674.2	52	21151.4	0.0	0.9	0.00	-129.2	-28.8
HKW 8-LMC 3	89.3	94.0	4.6	4.7	0.0	28754.0	45	18613.7	0.0	0.8	0.00	-113.7	-25.4
HKW 8-LMC 3	94.2	98.9	4.8	4.9	0.0	29745.4	47	19255.4	0.0	0.8	0.00	-117.6	-26.2
HKW 8-LMC 3	90.6	94.2	23.1	23.2	0.1	140857.9	223	91183.3	0.0	4.0	0.00	-556.9	-124.3
HKW 8-LMC 3	87.8	92.4	5.4	5.5	0.0	33635.6	53	21773.8	0.0	0.9	0.00	-133.0	-29.7
HKW 8-LMC 3	92.5	97.3	4.5	4.6	0.0	27754.9	44	17966.9	0.0	0.8	0.00	-109.7	-24.5
HKW 8-LMC 3	80.0	83.5	23.2	23.3	0.1	141307.7	223	91474.4	0.0	4.0	0.00	-558.7	-124.7
MKHD-W6-2	121.0	125.9	5.4	5.4	0.0	32674.2	52	21151.4		0.9	0.00	-129.2	-28.8
MKHD-W6-2	130	135.0	5.2	5.2	0.0	31705.4	50	20524.3		0.9	0.00	-125.3	-28.0
MKHD-W6-2	119	123.9	5.7	5.7	0.0	34589.7	55	22391.4		1.0	0.00	-136.7	-30.5
MKHD-W6-2	127.0	131.9	5.9	5.8	0.0	35536.6	56	23004.3		1.0	0.00	-140.5	-31.4
MKHD-W-6-1	87.0	102.1	26.0	10.0	16.0	123404.3	57754	39226.1	1.4	1.7	0.46	1284.5	2763.3
MKHD-W-6-1	88.0	103.2	26.1	9.1	17.0	122182.7	61256	35960.1	1.5	1.6	0.49	1397.3	2939.3
MKHD-W-6-1	85.0	100.0	26.0	9.4	16.6	122277.7	59883	36991.5	1.5	1.6	0.48	1354.6	2870.7
MKHD-W-6-1	89.0	103.7	24.3	16.2	8.1	130290.8	29397	63722.6	0.7	2.8	0.21	383.8	1341.7
MKHD-W-6-1	92.0	107.1	25.4	11.8	13.6	125176.5	48983	46570.9	1.2	2.0	0.38	1007.3	2324.0
MKHD-W-6-1	93.0	108.2	25.8	10.8	15.0	124461.3	54045	42531.7	1.3	1.9	0.42	1166.1	2577.2
MKHD-W-6-1	84.0	98.7	24.9	13.2	11.6	125987.1	41991	52036.0	1.0	2.3	0.32	788.8	1974.2
HKW 7-CZ2.1	56.0	59.3	19.2	19.0	0.1	115718.8	183	74909.7	0.0	3.3	0.00	-457.5	-102.1
HKW 7-CZ2.1	57.2	60.5	18.5	18.3	0.0	111256.4	176	72021.0	0.0	3.1	0.00	-439.8	-98.2
HKW 7-CZ2.1	58.0	61.3	20.1	19.9	0.1	121033.6	191	78350.2	0.0	3.4	0.00	-478.5	-106.8
HKW 7-CZ2.1	60.5	63.8	19.9	19.8	0.1	120077.3	190	77731.1	0.0	3.4	0.00	-474.7	-105.9
HKW 7-CZ2.1	57.0	60.3	19.0	18.9	0.1	114736.8	181	74274.0	0.0	3.2	0.00	-453.6	-101.2
HKW 7-CZ2.1	56.5	59.8	17.8	17.6	0.0	107186.9	169	69386.6	0.0	3.0	0.00	-423.8	-94.6
HKW 7-CZ2.1	55.5	58.8	18.5	18.3	0.0	111256.4	176	72021.0	0.0	3.1	0.00	-439.8	-98.2
HKW 7-CZ2.1	58.0	61.3	17.2	17.0	0.0	103534.2	164	67022.1	0.0	2.9	0.00	-409.3	-91.3
HKW 7-CZ2.1	57.2	60.5	17.3	17.2	0.0	104587.2	165	67703.8	0.0	2.9	0.00	-413.5	-92.3
HKW 7-CZ2.1	54.0	57.3	17.2	17.0	0.0	103534.2	164	67022.1	0.0	2.9	0.00	-409.3	-91.3
HKW 7-CZ2.1	55.0	58.3	19.0	18.9	0.1	114736.8	181	74274.0	0.0	3.2	0.00	-453.6	-101.2
HKW5-64-1	183.0	187.7	15.1	15.0	0.0	91364.7	144	59144.2		2.6	0.00	-361.2	-80.6
HKW5-64-1	191.0	195.6	16.2	16.2	0.0	98144.4	155	63533.0		2.8	0.00	-388.0	-86.6
HKW5-64-1	182.0	186.6	15.8	15.8	0.0	95925.1	152	62096.4		2.7	0.00	-379.2	-84.6
HKW5-64-1	156.0	160.3	17.9	17.9	0.0	108725.3	172	70382.5		3.1	0.00	-429.8	-95.9
HKW5-16-1	123.0	127.0	16.9	16.9	0.0	102473.2	162	66335.2		2.9	0.00	-405.1	-90.4
HKW5-16-1	128.0	132.1	17.9	17.8	0.0	108214.2	171	70051.7		3.0	0.00	-427.8	-95.5
HKW5-16-1	126.0	130.0	18.1	18.1	0.0	109742.6	173	71041.0		3.1	0.00	-433.9	-96.8
HKW5-16-1	130.0	134.1	16.7	16.7	0.0	101404.0	160	65643.1		2.9	0.00	-400.9	-89.5
HKW 7-Lam1.1	164.0	168.5	16.6	16.5	0.0	100326.3	158	64945.5	0.0	2.8	0.00	-396.6	-88.5
HKW 7-Lam1.1	164.0	168.5	16.2	16.2	0.0	98144.4	155	63533.0	0.0	2.8	0.00	-388.0	-86.6
HKW 7-Lam1.1	185.0	189.6	17.1	17.0	0.0	103004.7	163	66679.3	0.0	2.9	0.00	-407.2	-90.9
HKW 7-Lam1.1	196.0	200.7	15.2	15.1	0.0	91944.1	145	59519.3	0.0	2.6	0.00	-363.5	-81.1
HKW 7-Lam1.1	192.0	196.7	15.8	15.7	0.0	95364.1	151	61733.3	0.0	2.7	0.00	-377.0	-84.1

Table S1.5. LA-ICP-MS U-Th-Pb data report 1.

Laboratory & Sample Preparation	
Laboratory name	Laboratory for Environmental and Raw Materials Analysis (LERA), Karlsruher Institut for Technology (Germany)
Sample type/mineral	Carbonate
Sample preparation	Regular thin sections
Imaging	Petrographic microscope
Laser ablation system	
Make, Model & type	Analyte Excite+, Teledyne PhotonMachines ArF excimer laser
Ablation cell	HelEx 2-volume cell
Laser wavelength	193 nm
Pulse width	4 ns
Fluence	2 J/cm2
Repetition rate	10 Hz
Pre-ablation	5 pulses (same parameters as main ablation)
Ablation duration	18 s
Ablation rate	~ 0.8-1 μm/s
Spot shape & size	Round, 150 μm (65 μm and 85 μm for primary RM)
Sampling mode	Static spot ablation
Gasses	Sample cell: He. Funnel: He + Ar. Tubbing: He + Ar + N
Gas flows	He (300 ml/min, cell), He (200 ml/min, funnel), Ar (900 ml/min), N (12 ml/min)
ICP-MS Instrument	
Make, Model & type	ThermoScientific ElementXR sector field ICP-MS
Sample introduction	Ablation aerosol
RF power	1200 W
Detection system	Secondary electron multiplier (with conversion dynode at -8kV). Simultaneous analogue and counting (pulse) modes of detection (conversion factors calculated per mass and applied offline). Magnetic field fixed. Detection by peak jumping with electrostatic analyzer.
Masses measured	202, 204, 206, 207, 208, 232, 238
Dwell times	202: 3 ms, 204: 3 ms, 206: 18 ms, 207: 32 ms, 208: 9 ms, 232: 7 ms, 238: 12 ms
Samples per peak/integration type	3 for 202 and 204; 4 for the rest of masses
Total time per run	90 ms
Number of runs/total time	330 / 32.5 s
Acquisition mode	Trigger from laser (15 s after pre-ablation), background: 14.5 s, ablation: 18 s
Dead time	19 ns

Table S1.6. LA-ICP-MS U-Th-Pb data report 2.

Data Processing	
Gas blank	14.5 s on-peak zero subtracted.
Calibration strategy	- Primary RM: SRMNIST612 (Jochum et al., 2011) - Offset RM: WC-1 carbonate (Roberts et al., 2017) - Validation RM: JT-1 (Guillong et al., 2020), and B-6 (Pagel et al., 2018) carbonates
Data processing / LIEF correction	In-house VBA spreadsheet program (Gerdes and Zeh, 2006, 2009). Intercept method for LIEF correction, assumes Pbc corrected WC-1 and samples behave identically.
Mass discrimination	$^{207}Pb/^{206}Pb$ (-0.4/0-0.18/-0.09/0.36 %) and $^{206}Pb/^{238}U$ (23.69/24.23/18.7/20.79 %) normalised to primary RM (values for each of the sessions).
Common-Pb correction	No common-Pb correction applied
Uncertainty level & propagation	Uncertainties are quoted at 2s absolute and are propagated by quadratic addition of the within run precision, counting statistics, background, common Pb correction (if applicable) and the excess of scatter (calculated from the primary RM). In addition, in the session 4, an excess of variance of 0.49 % (1s), calculated from the offset RM, was added quadratically to the $^{206}Pb/^{238}U$ ratios. Systematic uncertainties are reported as an expanded uncertainty, considering long term reproducibility (1.5%, 2s) and decay constant uncertainties.
Quality control / Validation	Session 1 (Matrix offset = 0.88): WC-1: 254.0 ± 1.9 Ma (2s, MSWD = 0.46, n = 16) JT-1: 13.85 ± 1.44 Ma (2s, MSWD = 0.83, n = 16) B-6: 43.25 ± 0.92 Ma (2s, MSWD = 0.99, n = 16) Session 2 (Matrix offset = 0.895): WC-1: 253.6 ± 1.6 Ma (2s, MSWD = 0.69, n = 13) JT-1: 14.32 ± 0.98 Ma (2s, MSWD = 0.85, n = 14) B-6: 43.00 ± 0.77 Ma (2s, MSWD = 0.55, n = 14) Session 3 (Matrix offset = 0.985): WC-1: 254.0 ± 1.5 Ma (2s, MSWD = 0.83, n = 12) JT-1: 14.48 ± 1.19 Ma (2s, MSWD = 0.70, n = 12) B-6: 41.61 ± 0.86 Ma (2s, MSWD = 1.51, n = 12) Session 4 (Matrix offset = 0.96): WC-1: 254.0 ± 1.9 Ma (2s, MSWD = 1.0, n = 10) JT-1: 13.84 ± 0.97 Ma (2s, MSWD = 0.61, n = 12) B-6: 42.74 ± 0.80 Ma (2s, MSWD = 1.01, n = 12) Session 5: WC-1: 254.1 ± 2.2 Ma (2s, MSWD = 0.99, n = 14) B6: 42.64 ± 0.44 Ma (2s, MSWD = 1.02, n = 12) Duff Brown Tank: 64.31 ± 1.00 Ma (2s, MSWD = 1.70, n = 14) (Ages are the $^{206}Pb/^{238}U$ lower intercept ages of the calculated isochrons with the concordia curve in the Tera-Wasserburg space)